GLA-PPE 2001/04

arXiv:hep-ph/0109254 v1 26 Sep 2001

HEAVY FLAVOUR PHYSICS AT HERA – A SURVEY

P. J. BUSSEY
Department of Physics and Astronomy, University of Glasgow, Glasgow G12 8QQ, UK

Abstract
At the HERA collider at DESY, high energy electron and positron beams interact with proton beams. A review is presented of the variety of ways in which these collisions produce final states containing charm and beauty quarks.

1. Introduction

1.1. *The HERA collider*

The HERA collider is the only experimental facility in the world where high-energy electron-proton and positron-proton interactions can be studied. Electrons (or positrons) and protons are accelerated in the DESY ring complex to energies of 27.5 GeV and 920 GeV respectively (fig. 1a). The circulating beams are then brought to a focus at the two collision points where the H1 and ZEUS experiments are located. In most of the $e^{\pm}p$ interactions, the incoming $e^{\pm}$ interacts with the proton by first radiating a virtual photon (fig. 1b). The virtuality Q^2 of this exchanged photon (for definition see section 1.5) lies within a wide range; its minimum value is limited by the kinematics of the radiation process to be of the order of the electron mass squared, while its maximum value is limited to 10^5 GeV^2 by the energies of the incoming beams.

During the period 1992-2000, the H1 and ZEUS experiments each accumulated approximately 135 pb^{-1} of integrated luminosity, which has enabled a broad range of physics to be investigated. At low Q^2, the exchanged photon resembles a real photon, and we shall usually refer to such collisions simply as γp or "photoproduction". Real photons, as will be discussed below, can display hadronic as well as electromagnetic properties. The hadronic behaviour falls away over a transition region where Q^2 is of the order of 1 GeV^2, above which we are in the regime of deep inelastic scattering (DIS). Here the photon is primarily an electromagnetic object which couples to quark-antiquark ($q\bar{q}$) pairs. At very high Q^2 the exchange of Z and W bosons also becomes important. The $\gamma^* p$ luminosity is approximately uniform in $\log Q^2$, giving a prolific production of low-Q^2 photons.

Differences between e^+p and e^-p collisions are of significance in some new particle searches and at the very high Q^2 values where electroweak effects occur. In the physics reviewed here, however, the sign of the incoming e beam is nearly al-

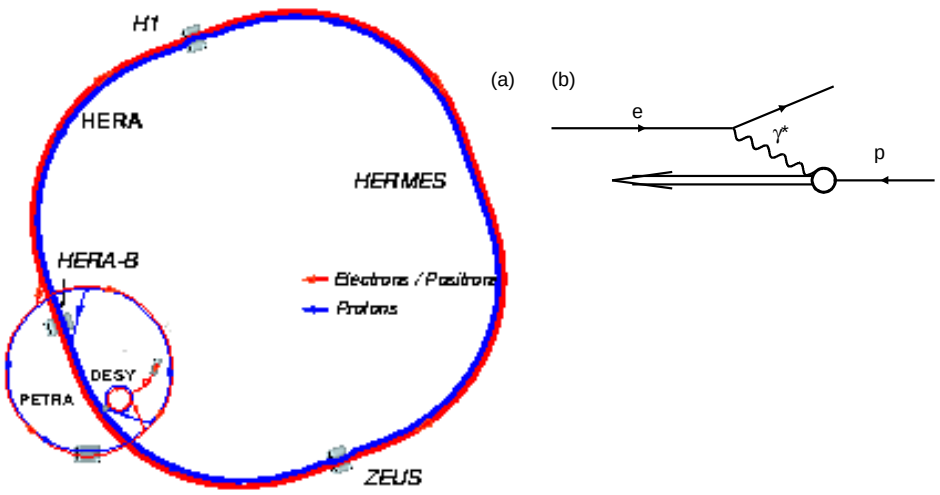

Fig. 1. (a) The HERA collider complex at DESY, showing the ep ring and the lower energy accelerator PETRA. The H1 and ZEUS experiments are in the North and South halls respectively. The proton beam energy was raised from 820 to 920 GeV at the end of 1998. (b) ep interaction mechanism through the radiation of a virtual photon. The broad arrow denotes the final-state products.

ways unimportant. For convenience, we shall normally refer to the incoming $e^{\pm}$ as a positron, including electrons by implication, since most of the integrated luminosity was taken with positrons. The symbol γ^* will denote any virtual photon, while γ will refer, where appropriate, to the particular case of low-Q^2, quasi-real photons.

1.2. *QCD physics with heavy quarks at HERA*

In the present survey, we consider those processes at HERA in which heavy flavours are produced, namely the production of particles containing charm (c) and beauty (b) quarks. HERA is *par excellence* a laboratory for the study of quantum chromodynamics (QCD), our present theory of the strong interaction. While e^+e^- colliders such as LEP have enabled the production of $q\bar{q}$ pairs to be studied in depth, along with the associated radiation of gluons, the presence of the proton in the initial state at HERA allows a wide variety of further QCD processes to be investigated. The incoming γ^*, with its range of virtualities, probes powerfully the partonic properties of the proton and the reactions initiated through the quarks and gluons of which the proton is a source.

Heavy quark production can also, of course, be studed in hadron-hadron colliders such as the Tevatron. However a virtual photon is a cleaner probe than a second high-energy hadron, and it is experimentally possible to trigger on photon-induced processes that occur down to lower transverse momenta, down to a few GeV.

The behaviour of QCD processes is governed by the running coupling constant α_s, whose value is $\approx$0.12 at momentum transfers corresponding to the Z mass,

though significantly higher at a few GeV. Consequently, the lowest-order (LO) perturbative calculations, which suffice to a first approximation, require frequently to be replaced by next-to-leading order (NLO) calculations or higher. This can present formidable technical difficulties, which can limit our experimental understanding of QCD. With light quark systems, a certain impasse may by now have been reached, but the consideration of b or c quarks presents a number of new factors. These arise because the production of a heavy object requires a corresponding momentum transfer which may be significantly higher than the QCD scale parameter $\Lambda_{QCD} \approx 300$ MeV. Such processes offer a different perspective on the operation of QCD. The measured final-state hadron containing a heavy quark relates directly to the properties of the QCD-governed hard scatter, and although the presence of a second momentum scale can complicate the theory, it provides a means of calculating cross sections using perturbative approaches that are unavailable, or less reliable, when dealing with exclusively light quark systems.

There remain a number of difficulties, however. The effective mass of the c quark is uncertain within the range 1.3 to 1.5 GeV, a value which is itself not overwhelmingly higher than Λ_{QCD}. These facts translate into significant uncertainties in the perturbative calculations, comparable to the effects of higher-order QCD diagrams. As will be seen, this makes the interpretation of many experiments less than straightforward. The higher mass (≈ 4.75 GeV) of the b quark should reduce these problems; nevertheless it will be seen that even the production of b hadrons currently presents challenges to theory.

A major aspect of heavy quark physics concerns the weak decays of the hadrons that contain these quarks. Such decays may be studied at any collider that is able to produce the relevant hadrons in sufficiently large numbers. Many of the most interesting decay channels have low branching ratios, however, and HERA has not yet produced data in enough quantity to be competitive here; CP violating effects, especially, lie in the domain of the B factories and the Tevatron. The present survey therefore concentrates on the production mechanisms of heavy flavour systems, an area where HERA is able to play a prominent role. The author's aim is to provide an account which is accessible to non-specialist readers and gives an up-to-date picture of the state of this area of HERA physics. Experimental results are preliminary where indicated.

1.3. *The H1 and ZEUS detectors*

The H1 and ZEUS detectors[1,2] are situated respectively at the north and south collision regions of HERA. Each detector comprises of a cylindrical central tracking chamber, surrounded by calorimeters. Both central tracking chambers are of drift chamber design. In the case of H1, the calorimeters consist of lead and steel converters in liquid argon, and are mainly located inside the solenoidal magnet which provides a magnetic field of 1.15 Tesla. In ZEUS, the calorimeter is a uranium-scintillator sandwich. It lies outside the solenoid, within which there is a field of 1.4 Tesla. The return yokes are part of the muon detection system, with muon detec-

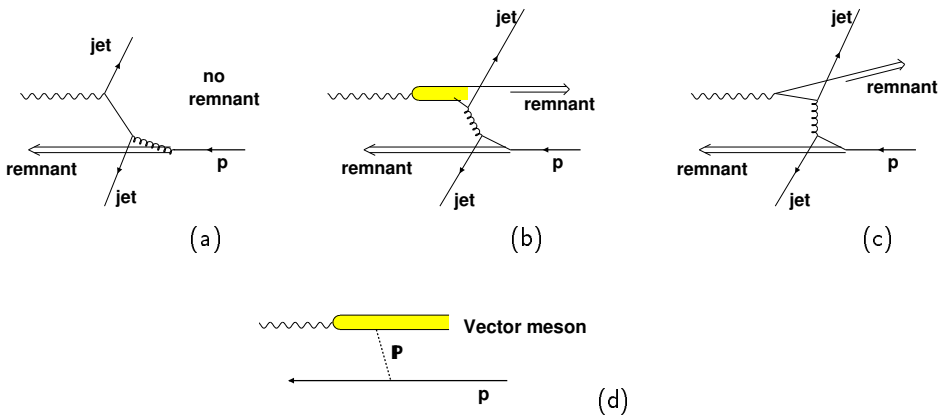

Fig. 2. Examples of different types of photon-proton interaction: (a) direct (b) resolved (c) anomalous (d) elastic diffractive.

tion arrays outside them. H1 has a silicon vertex detector array; ZEUS is currently commissioning its own silicon system.

Both detectors have a design which is approximately cylindrically symmetric around the beam line, but with a forward-backward asymmetry. In the forward (proton beam) direction there is a need for good hadron calorimetry in order to detect energetic particles associated with the proton, its remnants, and particles that are in general boosted in this direction. In the rear direction, the best possible electromagnetic calorimetry is required to measure accurately the deep inelastic scattered positrons.

In both experiments the calorimetry is designed to be as hermetic as possible, with holes of a minimum size for the beam pipes.

1.4. *Types of photon-hadron interaction*

Since the ep processes of concern here are mediated almost entirely by photons, some basic classes of photon-proton interactions must be considered. The most important of these are illustrated in fig. 2, where the first three diagrams depict different hard QCD scattering processes. *Direct* processes (a) are those in which the entire photon couples to a quark-antiquark line at high transverse momentum p_T. Alternatively (b), the proton may interact through an intermediate hadronic state which is a source of partons that can scatter off those in the proton. These are known as *resolved* photon processes, and here the photon possesses a parton structure like any other hadron. The concept of a resolved photon can be extended to situations where the photon couples to a relatively low-p_T quark pair (c). These perturbatively calculable processes are sometimes referred to as *anomalous* photon processes.[3]

Ultimately, the outgoing partons hadronise as jets or beam remnants. The signature for a resolved or direct photon process at LO is the presence or absence,

respectively, of a photon remnant in the event. The direct and resolved classes of photon interaction are fully distinct only in LO processes such as those illustrated. At NLO the two classes can still be defined for calculational purposes, but a continuum of diagrams exists connecting them. In photoproduction, the resolved processes occur at higher rates than the direct process, but as the Q^2 of the photon increases, the resolved cross sections decrease and the reactions become predominantly direct in nature.

The fraction x_γ of the incoming photon energy that enters a given QCD subprocess is an important parton-level quantity. In direct processes it is by definition unity, while in resolved processes it can take any value in the range (0,1). The parameter x_γ is clearly defined in LO diagrams but at higher order there can be ambiguities. Experimentally the hadronic final state is measured, and a suitable final-state quantity is required which correlates with x_γ in a chosen theoretical description of the process. For dijet final states, two such experimental estimators[4,5] are

$$x_\gamma^{\rm OBS} = \frac{\Sigma_{jets} E_T^{jet} e^{-\eta^{jet}}}{2E_\gamma} \qquad \text{and} \qquad x_\gamma^{meas} = \frac{\Sigma_{jets}(E-p_z)}{\Sigma_{event}(E-p_z)}.$$

Here as elsewhere E_T denotes transverse energy, namely $E\sin\theta$ for a single particle, summed over the particles in a jet. The laboratory pseudorapidity η is given by

$$\eta = -\ln\tan\frac{\theta}{2},$$

where θ is the polar angle and the proton beam defines the forward $(+z)$ direction. The proton has $E-p_z=0$ to an excellent approximation, and a quasi-real incoming photon has $E-p_z = 2E_\gamma = \Sigma_{event}(E-p_z)$. Snowmass — i.e. E_T-averaged — quantities[6] are used in $x_\gamma^{\rm OBS}$, while in x_γ^{meas} the sums are over all particles in the jets and in the event as a whole. One notes that for a massless object, $E_T e^{-\eta} \equiv (E-p_z)$; the two estimators differ in that $x_\gamma^{\rm OBS}$ neglects jet-mass effects. The estimator $x_\gamma^{\rm OBS}$ has been mostly used in HERA analyses.

A further class of processes in which $b\bar{b}$ and $c\bar{c}$ systems are produced comprises *diffractive* processes. An example is illustrated in fig. 2d, where the photon forms an intermediate vector meson state V which scatters off the proton by the exchange of a pomeron. Both quasi-real and highly virtual photons may take part in diffractive processes at HERA; these will be the subject of Section 6 of this paper.

1.5. *DIS kinematics*

Let the incoming and the scattered positron have four-momenta k and k' respectively. Then the exchanged photon virtuality is

$$Q^2 = -q^2 = -(k-k')^2 = 4EE'\cos^2(\theta_e/2), \tag{1}$$

where θ_e is the polar angle of the scattered positron relative to the proton beam direction. If the overall ep centre-of-mass energy is $s=(k+P)^2$, where P is the

proton four-momentum, then Bjorken x is defined as $Q^2/(2P \cdot q)$. The quantity

$$y = \frac{Q^2}{sx} = 1 - \frac{E'}{E}\frac{1-\cos\theta_e}{2}, \tag{2}$$

represents the virtual photon energy, as a fraction of the positron energy, in the proton rest frame.

The cross sections for unpolarised DIS can be expressed in terms of structure functions F_2 and F_1. It is usually valid to neglect the contribution from F_1; one then obtains:

$$\frac{d^2\sigma}{dx\,dQ^2} = \frac{2\pi\alpha^2}{Q^4 x}\left(1+(1-y)^2\right)F_2(x,Q^2) \tag{3}$$

in terms of the electromagnetic coupling constant α. The overall structure function will be denoted by F_2 and the structure function for charm-containing events by F_2^c

The $\gamma^* p$ centre-of-mass energy or, equivalently, that of the final-state hadronic system, is termed W.

2. QCD Aspects of Heavy Flavour Production

Perturbative methods in QCD calculations require the occurrence of a momentum transfer that is much greater than the QCD scale parameter Λ_{QCD}. We shall first outline an approach that is widely used in calculating heavy quark cross sections for processes involving a high-p_T scatter. Let a hadron H, containing a heavy quark of flavour h, be produced from two initial-state partons i, j. The cross section is then expressed as the product of two basic terms:

$$\sigma_{QCD}(ij \to hx)\; f(h \to H). \tag{4}$$

where σ_{QCD} is the perturbatively calculated QCD cross section, i.e. at the parton level. Here the symbol x denotes further parton-level products, and the fragmentation factor $f(h \to H)$ is the probability for h to fragment into H in an outgoing jet. The inclusive fragmentation probability for x is taken as unity; if we are interested in a particular final-state product X then a further factor $f(x \to X)$ is needed. All these quantities are kinematics-dependent.

In HERA physics, the initial-state partons i, j can be taken as quarks, gluons or the incoming photon itself. A parton distribution function (pdf), namely $f(p \to j)$, is required for the proton. In resolved photon processes, a pdf $f(\gamma \to i)$ must be supplied similarly to denote the probability that the photon gives rise to the quark or gluon i that interacts.

Finally, expressions of type (4) are summed over all the relevant parton states. Thus for direct inclusive photoproduction of a given D meson one can write

$$\sigma(\gamma p \to Dx) = \sum_{j,x} f(p \to j)\; \sigma_{QCD}(\gamma j \to cx)\; f(c \to D). \tag{5}$$

The following points need to be noted:

(i) The QCD term σ_{QCD} may be calculated at LO or to higher orders;

(ii) The assumption that a process may be split into separate terms in this way is known as *factorisation.* A given fragmentation factor or pdf is normally assumed to be independent of the perturbative QCD process $ij \to hx$, i.e. it is *universal.* A mention of factorisation usually implies universality.

(iii) The pdf's and fragmentation factors incorporate a variety of initial-state and final-state processes. For example gluon radiation may occur and, if sufficiently hard, might legitimately be regarded as constituting a higher-order QCD process. By imposing a *factorisation scale,* one defines up to what momentum transfers such a gluon or its products will still be called part of the proton structure or part of the jet.

(iv) In general, these are non-perturbative quantities and must be obtained either from models or from experimental measurement. The assumption of universality implies that a fragmentation factor measured in one experiment can be used correspondingly in another experimental context. The pdf's are usually obtained from fits to large collections of experimental data.

(v) As the order of the QCD calculation rises, the validity of the above assumptions becomes more questionable.

Behind the kind of scheme outlined above there lies the physical insight that hard processes take place over a shorter time-scale than soft processes. Thus the production of the heavy quark may be regarded as prior to, and physically distinguishable from, the subsequent slower hadronisation phase.

2.1. *Methods and models*

At this point we present some theoretical models and procedures which are in common use in the analysis of heavy quark production. Some further topics will be discussed later in connection with the specific areas where they are met.

- *PYTHIA, HERWIG.* These well-known Monte Carlo models can calculate a large variety of QCD processes at LO. Initial and final state leading-logarithm parton showers are incorporated to simulate certain kinds of higher order effect. Hadronisation is performed in two different ways. In PYTHIA,[7] colour strings are constructed between the final-state partons, and then hadronised according to a set of phenomenological prescriptions. In HERWIG,[8] a series of parton clusters are produced and allowed to decay. Both these models are extensively used, and form the basis of further models. The PYTHIA colour-string fragmentation is also known by the name of JETSET.

- *Peterson fragmentation model.* A standard representation of the fragmentation factor $f(h \to H)$, based on phenomenological considerations, is the Peterson formula:[9]

$$f(h \to H) \;=\; PD(z) \;=\; P\frac{A}{z\left[1 - 1/z - \epsilon/(1-z)\right]^2}, \qquad (6)$$

in which the hadron of interest, H, is produced at a given Feynman z relative to the momentum of the heavy quark h, with $z = (E + p_{||})_H/(E + p_{||})_h$ where $p_{||}$ denotes the momentum component along the h direction. A is a normalisation constant, and P is the total probability for h to fragment to H. The so-called Peterson parameter ϵ is determined from experiment:[10] a small value means that the fragmentation is peaked near $z = 1$. For c and b quarks, respectively, typical values of ϵ are 0.035 and 0.006. There is a question of whether the hadron is produced, on average, along the same direction as the quark, as taken in Peterson fragmentation, or whether the colour string from the proton remnant might pull the hadron to a higher rapidity (the "beam-drag effect"[11]). H1 have concluded that the effect is unimportant in DIS charm production.[12] On the other hand ZEUS[13] have obtained an improved description of charm rapidity distributions when the hadronisation procedure from JETSET or HERWIG is used in place of the Peterson method. These issues have been discussed further by Bodwin and Harris.[14] An analytic fragmentation function with possibly better relativistic properties is that of Bowler.[15] Others have been given by Kartvelishvili et al.[16] and Collins et al.;[17] see also the review by Frixione et al.[18]

- *Fixed flavour-number schemes.* In heavy quark production up to NLO, two main schemes have been proposed. In the *fixed flavour-number scheme,* often referred to in the charm case as the *massive charm* scheme, the incoming photon and proton are given hadronic structures which contain only three quark flavours (u, d, s). QCD interactions are then generated which produce heavy quark pairs ($q_h\bar{q}_h$), whose dynamics is calculated using a realistic quark mass assignment (e.g. $m_c = 1.5$ GeV). The heavy quark then fragments — e.g. using the Peterson formula — into an observable hadron. Since heavy quark excitation processes (see Section 3) are not treated, and may be important at high energies, these schemes are expected to work best at $p_T = O(m_h)$.

- *Variable flavour-number schemes.* To enable quark excitation to take place, charm and beauty are treated as active flavours in the proton or photon. In the more common *massless* ("zero-mass") versions, the mass m_h is treated as zero up to the final hadronisation which produces a massive H hadron. QCD processes taking place at $p_T \approx m_h$ may therefore not be accurately described, but this approach should work well at high p_T.

- *DGLAP evolution.* Given a set of pdf's or a structure function which apply at low Q^2, one may wish to know the corresponding quantities at higher Q^2 for a given Bjorken x value. The DGLAP equations[19] evaluate the necessary gluon radiations and splittings that occur in this transition, using perturbative QCD to a given order.

- *CCFM evolution.* As an alternative to DGLAP evolution, the CCFM scheme[20] uses a different form of factorisation in which parton densities are explicitly

treated as a function of transverse momentum (which is integrated over in the DGLAP treatment) and an angular ordering parameter is introduced. This is a development of the earlier BFKL evolution scheme,[21] which evolves amplitudes over x instead of Q^2 and claims advantages at small x. With CCFM there is a matched transition to the DGLAP regime; it is implemented in the CASCADE Monte Carlo among others.[22,23]

- *Parton distribution functions.* A variety of pdf's are on the market to describe the quark and gluon densities in the proton and the photon. They must be provided in versions suited to the order of the QCD calculation to which they are to be applied. In the case of the proton, the pdf's are usually obtained from fits to large collections of experimental data, and are updated when new experimental results are announced. The constraints of DGLAP evolution are normally applied. Two groups active in this area are CTEQ and MRST, whose publications may be consulted for further details.[24,25] In addition the H1 and ZEUS collaborations have calculated their own proton pdf fits on the basis of the DGLAP equations.[26,27]

  Photon pdf's are normally obtained based on the Vector Meson Dominance model (see Section 6), so that the partonic structure of the photon at low virtualities uses that taken for virtual mesons. An additional direct coupling of the photon to quark pairs ("box diagram") is included, and allowance is made for free parameters, such as the gluon density in the photon at low virtuality. Evolution in Q^2 from a base value Q_0^2 is performed. The models cited in the analyses quoted here, namely GRV,[28] GS,[29] AFG,[30] and SaS,[31] differ in a number of technical aspects, such as the value of Q_0, the factorisation scheme, treatment of heavy quark thresholds, and the number of free parameters that have been fitted to published data. The SaS model extends the pdf's to virtual photons. A review of some of the issues has been given by Vogt.[32]

3. Open Charm Production at HERA

The production of heavy quarks (q_h) in ep collisions takes place through three main mechanisms, which are here briefly outlined in turn:

In *photon-gluon fusion* (fig. 2a), the incoming virtual photon interacts with a gluon from the proton, so as to form an outgoing $\bar{q}_h q_h$ pair through the reaction $\gamma^* g \to q_h \bar{q}_h$. The LO diagram often offers a good description when the quark pair emerges at high p_T. The fusion process can give a direct measurement of the gluon content of the proton; this complements the determinations through QCD fits to the proton structure function F_2 as a function of Q^2. We shall refer to "photon-gluon fusion" in the context of photoproduction, and "boson-gluon fusion" in DIS, where γ^* and W/Z exchanges may both be present.

In *excitation* processes, the incoming γ^* interacts with a heavy quark that is an effective part of the proton structure and scatters it out of the proton. This may occur through resolved photon processes and through the direct "QCD Compton"

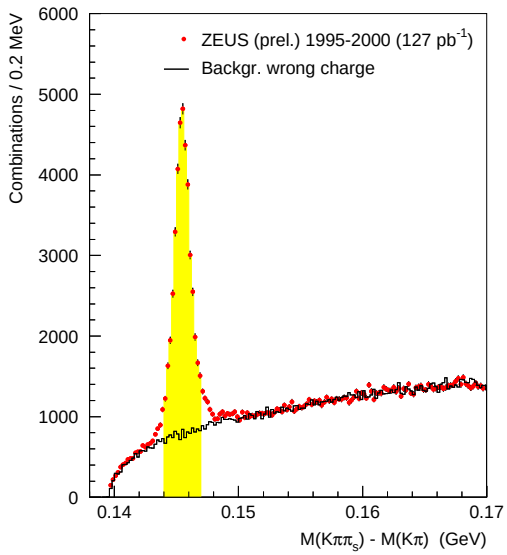

Fig. 3. $D^* - D$ meson mass difference, ΔM, illustrated from ZEUS photoproduction data (preliminary),[33] using $K\pi$ pairs selected to have invariant masses in the range 1.83-1.90 GeV.

process, $\gamma^* q_h \to g q_h$, whose cross section is somewhat smaller than that of the fusion process. The proton has only light valence quarks, and so any c or b content in its pdf is generated by DGLAP evolution — specifically, through a gluon fluctuating into a $q_h \bar{q}_h$ pair. Similar considerations apply to the photon.

In production by *fragmentation,* the heavy quark is found in a jet that originated from a light parton: specifically, an outgoing gluon splits into a $c\bar{c}$ or $b\bar{b}$ pair. Fragmentation may be treated entirely phenomenologically, obtaining the distributions from fits to data, or it may be calculated in perturbative QCD, e.g. in the process $\gamma q \to gq$ with $g \to q_h \bar{q}_h$, namely "gluon splitting". This is a higher order QCD process than the LO fusion term $\gamma g \to q_h \bar{q}_h$,.

The distribution of an observed hadron H in a jet requires in any case a phenomenological treatment of the hadronisation process.

3.1. *Charm meson states*

The lowest charm states are the cd and cu D^0 and $D^\pm$ mesons, which are produced along with excited states such as the D^*. The D^* mesons are easier to identify because of their decays to the D states through emission of a pion that is almost at rest relative to the D^*. The decay chains $D^{*\pm}(2010) \to D^0(1864) + \pi^\pm$, with $D^0 \to K^\mp \pi^\pm$ or $D^0 \to K^\mp \pi^\pm \pi^+ \pi^-$ (+ c.c.) are commonly selected since all the final state particles are charged, and hence accurately measurable. A typical mass-difference plot is shown in fig. 3. No peak is seen in the distribution that uses the wrong-sign combinations: this quantifies the background to the signal.

In recent ZEUS photoproduction data, the D^0 has been measured both as the

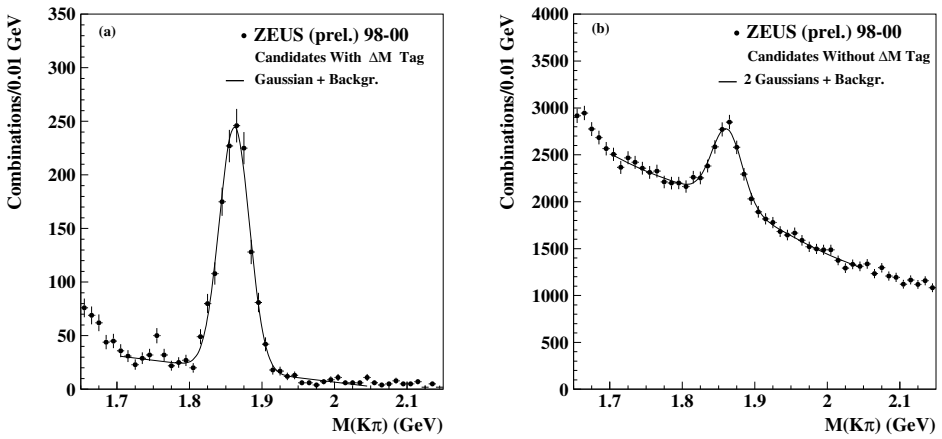

Fig. 4. ZEUS data (preliminary) on D meson production from $K^{\mp}\pi^{\pm}$ pairs (a) accompanied by an extra pion giving a mass difference ΔM consistent with D^* decay, (b) without an extra pion of this type.

product of D^* decay and in direct production.[34] Figure 4 shows the $K\pi$ mass distributions for these two cases. After selection on the ΔM peak, a dramatic D^0 signal is seen, while the directly-produced D^0 signal lies on a much higher background, although the number of events in the peak is much larger. In the latter case the wrongly-assigned $K\pi$ combinations remain in the plotted background. From these plots, ZEUS have evaluated the ratio $P_v = V/(V+PS)$ representing the production of the vector D^* (spin-1) relative to the pseudoscalar D. This is predicted to be 0.75 from simple spin statistics, but the inclusion of decays from heavier charm states and the effects of hadronisation can reduce this value. ZEUS obtains the value $P_v = 0.546 \pm 0.045 \pm 0.028$ (preliminary),[35] in agreement with measurements at LEP.*

Other mesons with a single c quark are also observed at HERA. The cs system has as its lowest state the $D_s^{\pm}(1969)$ which has been detected by ZEUS in its $\phi\pi^{\pm}$ decay mode (fig. 5a).[36] Details of the production characteristics will be discussed below. The ratio of the cross sections for $D_s^{\pm}$ and $D^{\pm *}$ production can give a measure of the strangeness-suppression ratio, a phenomenological parameter of the Lund string fragmentation scheme. The cross section ratio is found by ZEUS to be $0.41 \pm 0.07^{+0.03}_{-0.05} \pm 0.10$(b.r.), where the last error is the uncertainty on the $D_s \to \phi\pi$ branching ratio. This value is in close agreement with the corresponding result from e^+e^- data. It corresponds to a strangeness-suppression ratio of $0.27 \pm 0.04^{+0.02}_{-0.03} \pm 0.07$(b.r.), in agreement with most other experiments and with the standard default value of 0.3 in JETSET. Both these and the above results support the concepts of factorisation and universality in charm fragmentation.

A further charm state recently reported by ZEUS is the $D_{s1}^{\pm}(2536)$, which decays

*Here and elsewhere, unless otherwise stated, the first of two quoted uncertainties is statistical and the second is systematic.

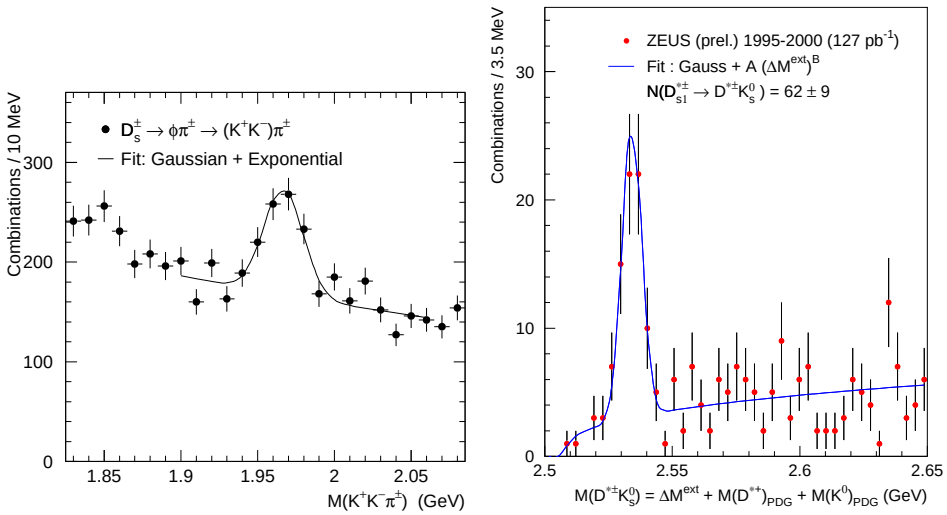

Fig. 5. ZEUS data on cs meson photoproduction: (a) $D_s^\pm(1969)$ signal seen in the decay $D_s^\pm \to \phi\pi^\pm \to K^+K^-\pi^\pm$ (b) $D_{s1}^\pm(2536)$ signal seen in the decay $D_{s1}^\pm \to D^{*\pm}K_S^0$ with $D^{*\pm} \to D^0\pi^\pm$ and $D^0 \to K^\mp\pi^\pm$ + c.c. (preliminary). The ΔM between the states before and after the K_S emission is added to the standard mass values of the decay products.

by emission of a K^0 meson to a $D^{*\pm}$.[33] This is one of a cluster of $L = 1$ states of the cs system. A clear signal is seen in photoproduction, (fig. 5b). The production rate and helicity characteristics are consistent with other measurements.[37] Evidence for the detection of other P-wave charm meson states has also been presented by ZEUS.[38] These are neutral states in the mass range 2.4 to 2.5 GeV. Further statistics are required to clarify the observations.

3.2. *Inclusive photoproduction of open charm*

ZEUS have published a study in which inclusive differential cross sections for $D^{*\pm}$ are compared with several "massive" and "massless" charm schemes in NLO QCD.[39] The $K\pi\pi\pi$ decay channel of the D provides a check on the higher-quality measurements using $K\pi$. The massive charm, fixed flavour-number scheme of Frixione et al. (FMNR)[40] is taken with several values of the Peterson fragmentation parameter ϵ, along with the massless, variable flavour-number calculations of Kniehl et al.[41,42] and of Cacciari et al.[43,44] The two massless calculations differ in the factorisation schemes applied to the fragmentation.

The shape, although not the normalisation, of the p_T distribution of the $D^{*\pm}$ is fairly well described by all the models, although the description cannot be said to be perfect (fig. 6). The issues have been recently discussed by some of the theoretical authors.[45] Pronounced differences, however, appear in the η distributions; these are shown in fig. 7a 7d integrated over p_T from different thresholds. In the highest p_T range (d), the scheme of Kniehl et al.[42] is more successful than that of Cacciari et al.,[44] whose predictions are too low. Although the latter scheme does appear to

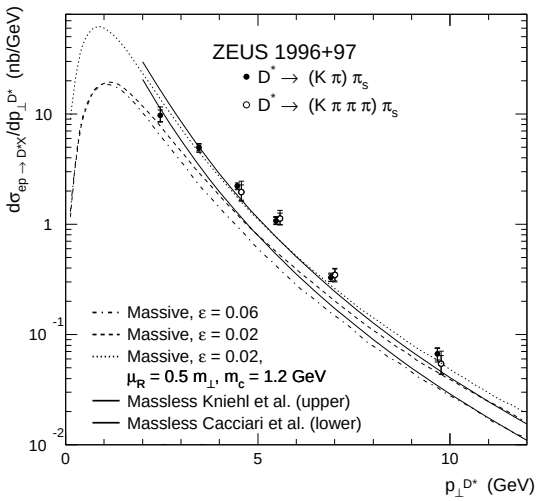

Fig. 6. D^* photoproduction: ZEUS distributions in p_T compared with models (see text). Outer error bars are statistical + systematic combined in quadrature; an overall normalisation uncertainty of $\pm 4\%$ is not shown. Note that the data here and in the next figure are quoted as ep cross sections.

work in the lowest p_T range measured (a), this is probably of little significance since neither massless calculation is appropriate for $p_T \approx m_c$. In fact even the massive scheme can be brought to reasonable agreement only by the artificial recourse of setting m_c as low as 1.2 GeV, while the massless schemes are unconvincing for $p_T < 6$ GeV.

Differences at the 20-25% level can be made by varying the photon pdf, as illustrated in fig. 7e - 7h, where (e), (g) use the calculation of Kniehl et al. and (f), (h) use that of Cacciari et al. For $p_T < 6$ GeV, the GS-G photon structure gives better results for the Kniehl et al. calculation due to its high c quark density, similar to that of the u quark. Since the quasi-real photon is believed to couple mainly to light-quark hadronic states, this structure may lack plausibility. It cannot, of course, be used in the massive-charm, fixed three-flavour-number scheme.

Overall, the message from these results is that the massive scheme has trouble between 3 and 6 GeV, where its chances of working are best, while the massless scheme of Kniehl et al. does seem to become more successful as p_T increases: higher p_T measurements are required to confirm this trend. Results from H1[46] have also been compared with the massive and massless charm calculations of FMNR[40] and Kniehl et al.[42] Cross sections as a function of laboratory rapidity are shown in fig. 8. At low p_T the results are qualitative similar to those of ZEUS, but at high p_T the data lie significantly above the calculations, in strong contrast to those of ZEUS. There are apparent differences between the two experiments here which need explanation.

Measurements of D_s production give further comparisons with theory. In fig. 9a, ZEUS first compare their data,[36] together with the previous D^* data,[39] with

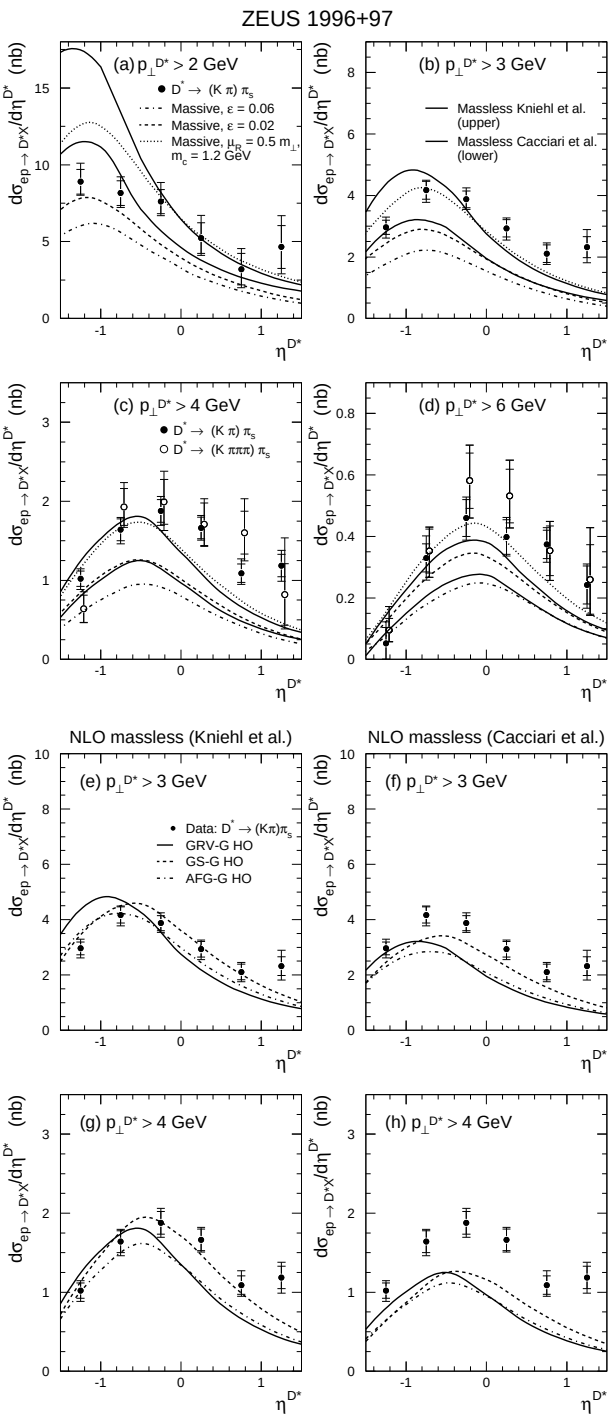

Fig. 7. D^* photoproduction: ZEUS pseudorapidity distributions compared with models (see text). Details as fig. 6; ep cross sections are given. GRV-HO photon pdf's are used in (a)-(d) and in the previous figure.

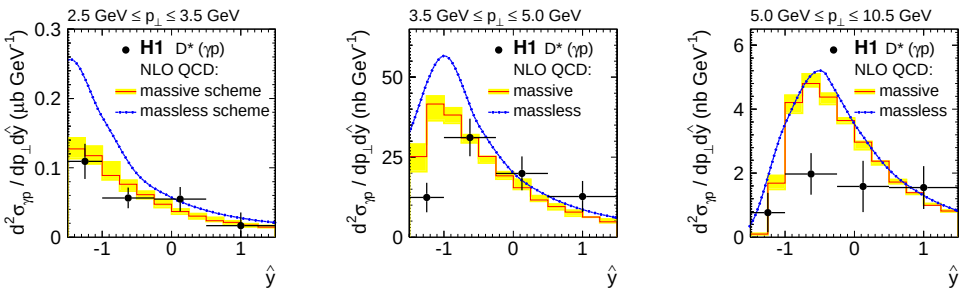

Fig. 8. Inclusive $\gamma p \to D^*$ cross sections from H1 vs. laboratory rapidity, compared with "massive" and "massless" models (see text). The shaded bands indicate variation of m_c between 1.3 and 1.7 GeV.

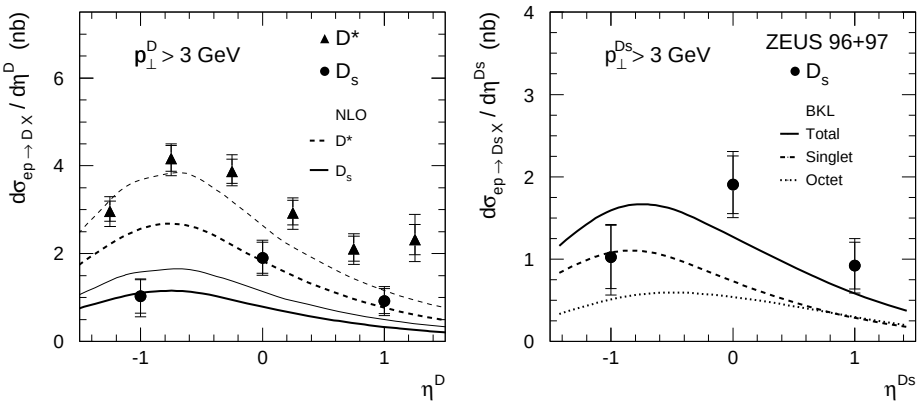

Fig. 9. Differential cross sections for inclusive D_s production (ZEUS) In the left-hand plot, the upper (thinner) curves of each type have $m_c = 1.2$ GeV and the lower (thicker) have $m_c = 1.5$ GeV. The BKL calculation (right) uses $m_c = 1.5$ GeV.

the FMNR model at NLO. The fragmentation to the D states was performed with a Peterson formula: the $f(c \to D^{*\pm})$ and $f(c \to D_s)$ distributions then differ by a simple scale factor. As discussed above, a standard calculation (heavy curves) fails to fit the D^* data although a low m_c value will almost suffice. The D_s data are consistent with this, but the statistics are at present poor. Another type of theoretical model has been given by Berezhnoy et al. (BKL),[47] who relate the experimental value of $f(c \to D^{*\pm})$ to $f(c \to D_s)$ by tuning the colour-singlet and colour-octet contributions to a description of the hadronisation. The $D^{*\pm}$ data are used to obtain the relevant singlet/octet ratio, yielding a prediction for the D_s cross sections. If both components are used, there is a fair description of the ZEUS data.

3.3. *Charm in dijet photoproduction*

More information can be obtained if the charm meson is associated with the production of jets. ZEUS have presented two analyses on this topic; note that at present, the inclusive D^*-containing events are measured with a defined experimental accep-

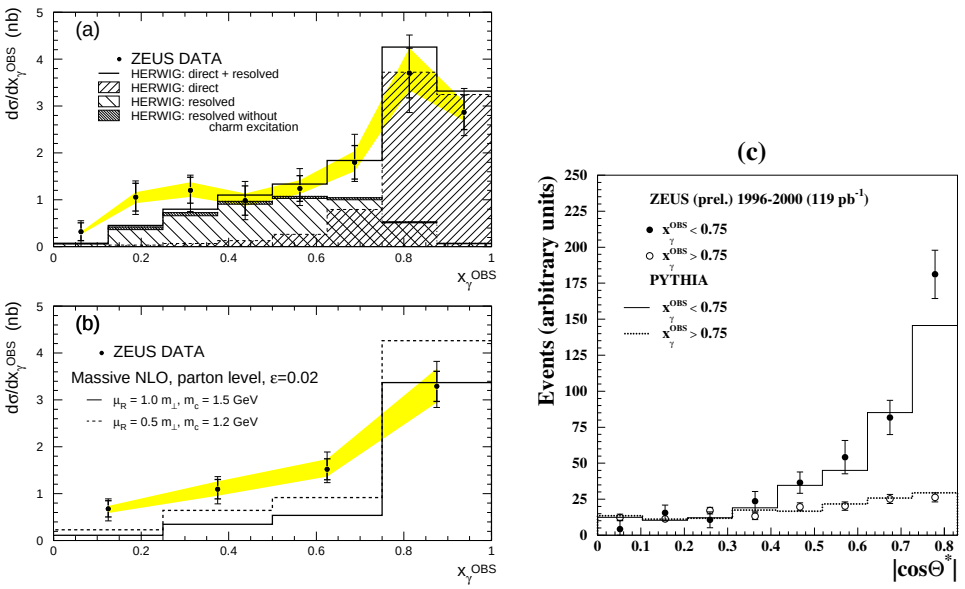

Fig. 10. Differential cross section $d\sigma/dx_\gamma^{\rm OBS}$ for dijets with an associated D^* meson: (a) ZEUS 96-97 data[39] compared with resolved and direct contributions calculated at LO using HERWIG; (b) (rebinned) data compared with NLO model of FMNR[40]. Jets with $E_T > 6$, 5 GeV and D^* with $p_T > 3$ GeV are used. (c) Distribution in $|\cos\theta^*|$, using increased data sample and jets with $E_T > 5$ GeV.[48]

tance, but with no specific association of the D^* with a jet, or information about a second charm particle in an event. The two highest-E_T jets found in an event are used. In fig. 10a, the distribution in $x_\gamma^{\rm OBS}$ is compared with predictions obtained using HERWIG, the total predictions of the model being normalised to the data. To a first approximation, HERWIG describes the shape of the distribution well, despite the QCD calculation being basically at LO. Above $x_\gamma^{\rm OBS} \approx 0.75$ a strong direct peak is seen both in the data and the theory. A strong resolved contribution is required. The tail to lower $x_\gamma^{\rm OBS}$ of the HERWIG direct contribution can be attributed to effects of hadronisation and initial-state gluon radiation. The small contribution of D^*'s arising from b quark production and decay is included.

To obtain this reasonable description of the resolved component, the GRV-G HO photon pdf was used.[28] This has given good results in many photoproduction analyses at HERA. It is possible to separate between the charm-excitation and the other charm contributions (e.g. $gg \to c\bar{c}$) in the HERWIG resolved calculation; the latter contributions are very small. The charm-excitation here is believed to come mainly from the photon: its nature is discussed further in section 3.5. The charm excited from the proton ends up mainly at forward angles outside the present experiments' acceptance.[49]

A parton-level comparison with the massive NLO calculation of FMNR is unsuccessful (fig. 10b). There is no explicit charm excitation in this calculation, by

definition, and three-flavour pdf's are used. The size of the direct peak is accurately accounted for, bearing in mind that gluon radiation pushes some of the events of direct origin into the low-$x_\gamma^{\rm OBS}$ tail. The effects of hadronisation would further increase this tail but are estimated to be small. So it is clear that the low-$x_\gamma^{\rm OBS}$ data are not described by the FMNR model, even with the desperate recourse of putting $m_c = 1.2$ GeV, which would anyway tend to spoil the agreement in the direct peak. This suggests as a conclusion that the fixed flavour-number scheme is inadequate in the context of charm photoproduction at moderate p_T.

This work has been extended by ZEUS, this time using PYTHIA as the reference Monte Carlo, in a study of dijet angular distributions in D^*-containing events. The direct process proceeds by quark exchange, while the resolved processes have a mixture of exchanges dominated by that of a gluon. These are respectively spin-$\frac{1}{2}$ and spin-1 exchanges, which have very different distributions in the scattering angle θ^* in the dijet rest frame. Experimentally they can be distinguished, to a reasonable approximation, by comparing the direct-dominated and resolved-dominated event samples with $x_\gamma^{\rm OBS} > 0.75$ and < 0.75 respectively.[48]

Preliminary results in fig. 10c show a steep angular rise in the direct-dominated events, in marked contrast to the gentler behaviour of the resolved-dominated events. The agreement with expectations is very satisfactory considering that the calculations are at LO. A next logical step will be to tag the jet with which the charm is associated, and examine the forward and backward distributions of the charm-tagged jets in the two classes of event, in order to study charm excitation in the photon and in the proton in more detail.

3.4. *Open charm in DIS*

The production of charm in DIS processes is dominated by the LO boson-gluon fusion diagram. Both HERA collider experiments have measured the inclusive production of the $D^{*\pm}$ in DIS and have used this to measure F_2^c, the part of the proton structure function F_2 which represents charm production. The method employed is to identify the $D^{*\pm}$ signal, correct it to an inclusive $D^{*\pm}$ production cross section in bins of x and Q^2, and then use a theoretical model to relate the $D^{*\pm}$ cross section to F_2^c, defined at the parton level. One writes:

$$F_2^{c\ exp}(<x>,<Q^2>) = \frac{\sigma^{exp}(x,Q^2)}{\sigma^{theor}(x,Q^2)}\ F_2^{c\ theor}(<x>,<Q^2>), \qquad (7)$$

to obtain an experimental F_2^c result at bin-averaged values of x, Q^2. The theoretical terms take account of the heavy quark fragmentation and the finite phase-space acceptance of the cross section measurement. The cross sections are taken to be sufficiently smooth-varying so that bin migration effects can be neglected.

H1 seek to compare their results with predictions from a DGLAP-based evolution scheme and also from a CCFM-based scheme.[12] To do this, they first make use of the hadronising LO Monte Carlo AROMA[50] to evaluate inclusive $D^{*\pm}$ cross sections from the observed event numbers. They then perform the subsequent calculation of

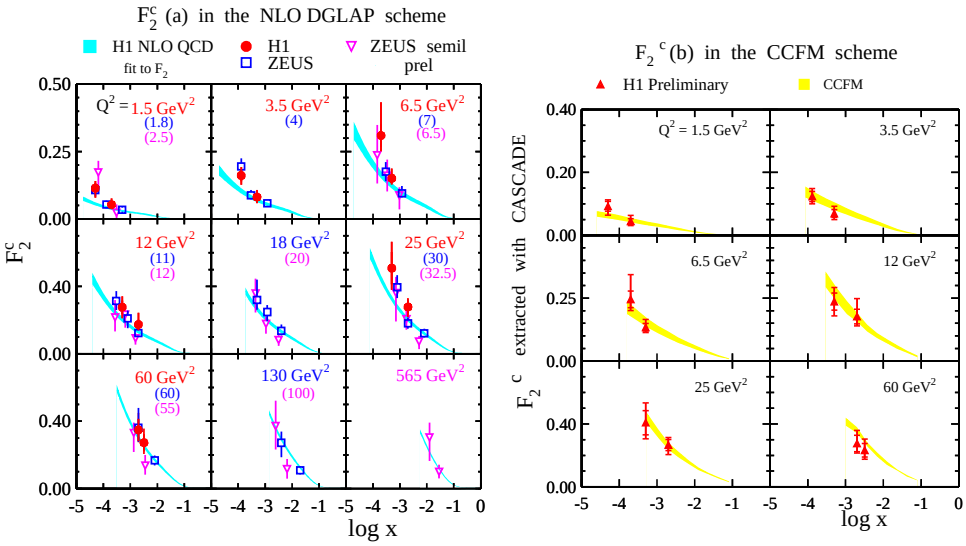

Fig. 11. Structure function F_2^c (a) measured by H1 and ZEUS using an NLO DGLAP scheme to correct to full phase space and (b) by H1 using a CCFM-based scheme. The preliminary results are compared with the respective theories. The shaded band represents the uncertainty on the c quark mass (1.3 - 1.5 GeV). Note that the ZEUS and H1 data are not at identical Q^2 values.

F_2^c in two ways, by means of (a) HVQDIS, which uses DGLAP, and (b) CASCADE, which uses CCFM. The HVQDIS program[51] uses a fixed flavour-number model for DIS in which the boson-gluon fusion process is calculated to NLO. The phase-space acceptance correction differs significantly in the two approaches, and so H1 have presented two different sets of experimental structure functions (fig. 11), each compared with the absolute predictions of a theory of a type similar to that used to perform the correction. The CCFM prediction includes proton gluon densities measured by H1 in an overall F_2 determination using this model. The shaded band represents the effect of varying the c mass between 1.3 and 1.5 GeV, which is the dominant uncertainty, and in the CCFM case the effect also of using a proton gluon density obtained with an NLO fit to F_2.

Overall, the CCFM-based calculation describes the data better than the NLO-DGLAP based calculation,[52] the differences appearing at lower values of Q^2 and x. Similar conclusions were obtained when comparing the inclusive $D^{*\pm}$ cross sections with these two models.

In a like manner, ZEUS have obtained $D^{*\pm}$ cross sections using RAPGAP to evaluate the hadronisation corrections and HVQDIS as the parton-level model.[13] The inclusive cross sections agree well with H1 and with HVQDIS, but a JETSET-style fragmentation function is required, rather than the Peterson formula, to perform the hadronisation corrections. There are some further technical differences from the H1 approach. ZEUS also find good agreement between their F_2^c measurements and results from an NLO QCD fit using ZEUS proton pdf's.[53] This is

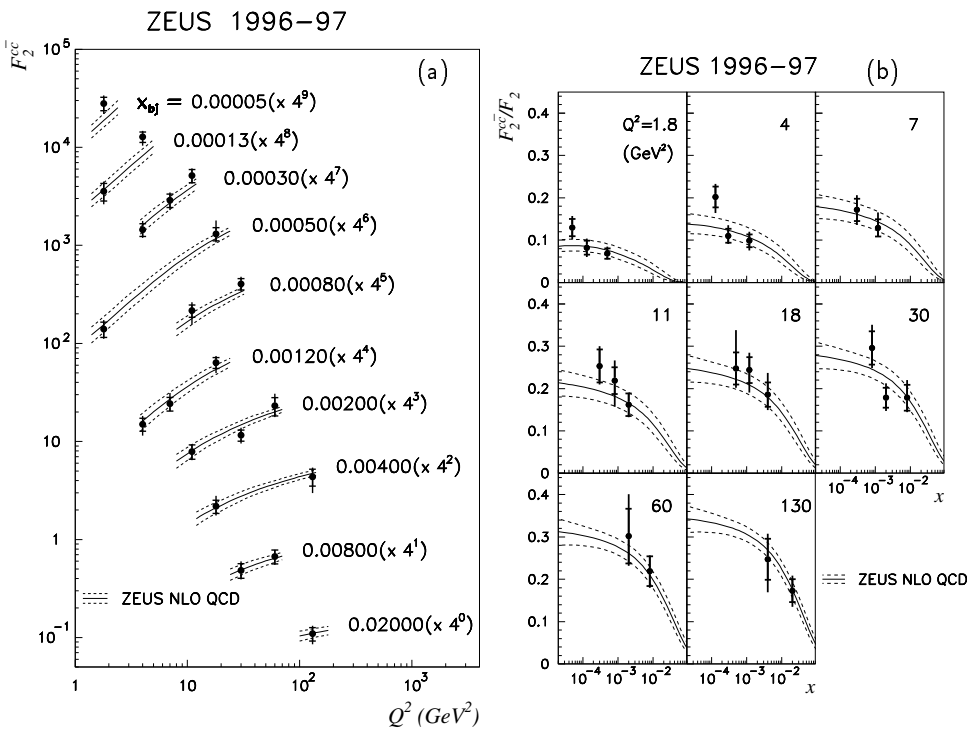

Fig. 12. (a) Charm structure function measured by ZEUS using an NLO DGLAP scheme to correct to full phase space, and compared with a fit using this scheme.[13] Uncertainties of around ±10% in the normalisation due to the luminosity measurement, the charm meson branching ratios and the charm fragmentation function are not included. (b) The ratio of the charm structure function to the total structure function F_2.

illustrated in the F_2^c results plotted as a function of Q^2 (fig. 12a) for different values of x. The variation of F_2^c with Q^2 — namely, scaling violation — is very much in evidence, and is well described globally by the theoretical fit. The uncertainty on the theory (dashed lines) is dominated by that on the c quark mass.

The ratio of F_2^c to F_2 is presented by ZEUS in fig. 12b. The fraction of charm events is substantial, owing to the flavour-insensitivity of the boson-gluon fusion process at high p_T. The flattening of the theoretical ratio as x becomes smaller is a feature of the boson-gluon fusion model: the rising charm production follows the rising gluon density in the proton, accompanying the similarly rising quark density which steers F_2. At high x this mechanism should fail, since the gluon density falls off and the proton has no charm valence quarks. The experimental data are consistent with these theoretical expectations. Overall, therefore, a clear physical picture seems to emerge.

Using a larger event sample from the period 1998-2000, ZEUS have confirmed that HVQDIS gives a good overall description of the $D^{*\pm}$ production, up to Q^2 values of 1000 GeV^2.[54] An unexpected observation is apparent in the preliminary

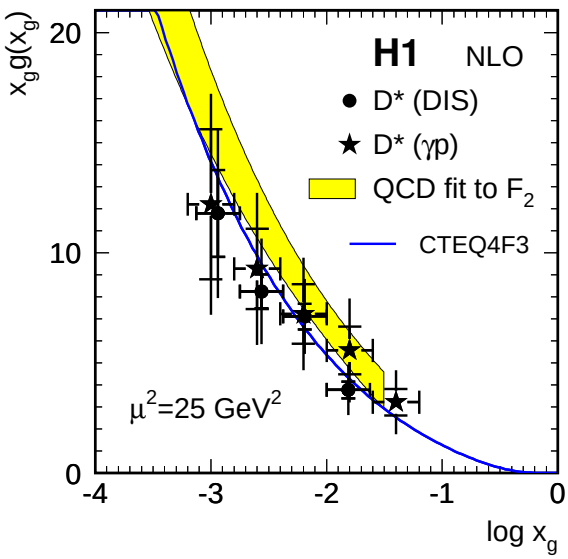

Fig. 13. Proton gluon densities obtained from two D^* analysis by H1, namely from photoproduction and from DIS, compared with the gluon density extracted from a QCD fit to F_2 data.

results, namely that the cross sections measured using an incoming electron beam are higher than those using a positron beam, although both sets individually remain consistent with HVQDIS. The effect appears highest at high Q^2. No explanation for the difference is yet on offer, and further investigation is required.

H1 have also extracted the gluon density in the proton on the basis that the charm production cross sections are dominated by the boson-gluon fusion process, and hence depend strongly on the proton gluon content. Results[46] using D^* data from photoproduction and DIS are plotted in fig. 13 and are compared with those from a QCD fit to F_2 data. The F_2 measurements depend primarily on the coupling of the virtual photon to quarks in the proton, with the DGLAP equations generating the gluon distribution in the course of the fitting procedure. The excellent agreement seen between the two types of method represents a significant triumph for the standard QCD description of the ep system.

3.5. *Photoproduction-DIS relationship*

To probe the nature of the charm process further, ZEUS have compared the production of charm in DIS with that in photoproduction.[55] Dijet events containing a $D^{*\pm}$ meson are selected, for $Q^2 \approx 0$ and in the range 1.0 to 5000 GeV^2. A value of $x_\gamma^{\rm OBS}$ is calculated for each such event, from which the authors evaluate the cross section ratio between events in $x_\gamma^{\rm OBS}$ below and above 0.75, i.e. an approximate "resolved/direct" ratio. This is plotted as a function of Q^2, and compared with theoretical predictions in fig. 14. The effects of uncertainties in the proton pdf largely cancel in taking this ratio, so that we are mainly looking at the properties of

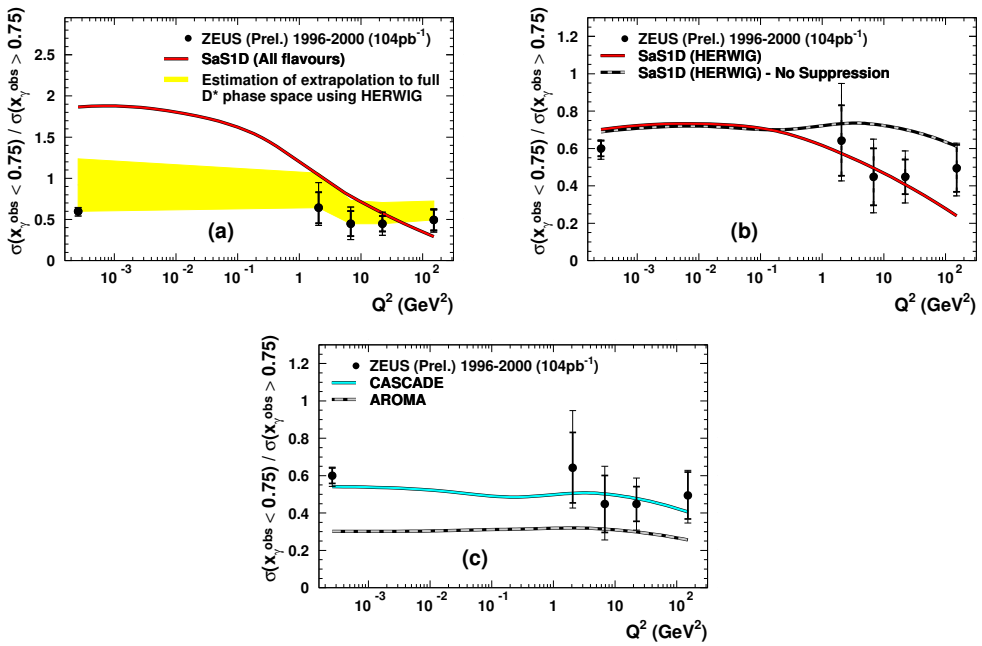

Fig. 14. Ratio of low to high $x_\gamma^{\rm OBS}$ cross sections of dijet events containing a D^* as measured in ZEUS (preliminary). Jet pairs with $E_T > 7.5$, 6.5 GeV are chosen, and D^* with $p_T > 3.0$ GeV. The results are compared with (a) HERWIG prediction calculated with no charm requirement. The possible effect of acceptance corrections is indicated. (b) HERWIG (with charm requirement) using the SaS1D photon structure with and without suppression of the photon parton structure with Q^2, (b) CASCADE and AROMA,

the photon. The ratio is found to be approximately constant with Q^2, a behaviour which contrasts strongly with that found in events lacking a charm requirement, and which cannot be accounted for by acceptance effects. Such behaviour is predicted by the Monte Carlos HERWIG, CASCADE and AROMA. With HERWIG, the SaS-1D photon pdf's were used with and without the option of suppressing the hadronic photon contribution with increasing Q^2; however, the data are not yet able to distinguish between these cases. The AROMA prediction is flat, but quantitatively too low, while CASCADE gives a good overall description.

These observations are consistent with the expectation that, after factorising out the proton pdf, the resolved photoproduction of charm takes place mainly through perturbative QCD mechanisms as does the direct process. Thus the "resolved/direct" ratio should not vary rapidly with Q^2. This contrasts with the non-perturbative, hadronic processes which dominate light-quark resolved photoproduction and which show a strong fall-off with Q^2. In other words, we are talking about "anomalous" diagrams here, rather than about a charm-containing hadronic photon structure.

Nevertheless, further statistics are clearly required to distinguish between the two SaS models, and data at higher Q^2 will also help.

3.6. *Some theoretical comments*

The HVQDIS model gives good results, but neglects the intrinsic charm that can evolve in the proton, in other words charm excitation processes, and so could have problems for Q^2 values above the charm mass squared. However the experiments do not yet seem to be sufficiently precise to be sensitive to such an effect. Also, HVQDIS does not attempt to describe $c\bar{c}$ formation from the splitting of outgoing gluons, and the formation of final-state J/ψ mesons has been ignored in these measurements; this contribution is not believed to be at an important level.

Given the merits and drawbacks of the existing fixed and variable flavour-number schemes, one might obviously wish for a more advanced type of scheme that combines the advantages of both. This would require a model which allows the number of active flavours in the proton and photon to vary with Q^2 or E_T, while also treating the charm quark mass satisfactorily. In a composite approach, each of the previous schemes will dominate in its own particular dynamic range, while a suitable "matching" is achieved in the intermediate region. A LO model of this type was provided by Aivazis et al. (ACOT).[56] Further developments have been presented by Collins,[57] who showed that the ideas can be made to work at all orders, and by Amundson et al. (ASTW),[58] who report a program of calculations at NLO. The latter authors provide a Monte Carlo program which can be used by experimentalists. At present ASTW are able to give a good account of the HERA F_2^c measurements. Their procedure is less successful with the differential inclusive charm meson distributions, owing to a strong sensitivity to an internal scale parameter within the model; good qualitative agreement is obtained with the data, but the theoretical uncertainties are very large. ASTW state an intention to extend their calculations to higher order.

There are a number of further implementations of these ideas. This approach offers a conceptually attractive way forward to a deeper understanding of charm production, provided that a sufficiently high order calculation can be achieved. In principle it should be applied also to beauty production.

It has been pointed out by Chuvakin et al.[59] that the fixed flavour-number schemes at NLO are very stable as regards scale variations, and are therefore well suited for the description of DIS processes over a wide Q^2 range. On the other hand, the cross sections contain large logarithms of the form $\ln(Q^2/m^2)$, and these can be resummed in a variable flavour-number scheme, where the problematic terms can be absorbed into the pdf's. These authors demonstrate that variable flavour-number schemes (BMSN[60] and CSN[61]) are able to give good descriptions of D^* production at HERA. However the results of the calculations are very similar to the fixed flavour-number calculations of HVQDIS. In view of the latter's moderate scale dependence, there may be at present no advantage in moving to the other schemes, at least insofar as the Q^2 and x description is concerned.

It should finally be remarked that considerable care is required in defining F_2^c at the theoretical level.[24] For a further discussion of some of the theoretical issues, the account by Harris[62] may be consulted.

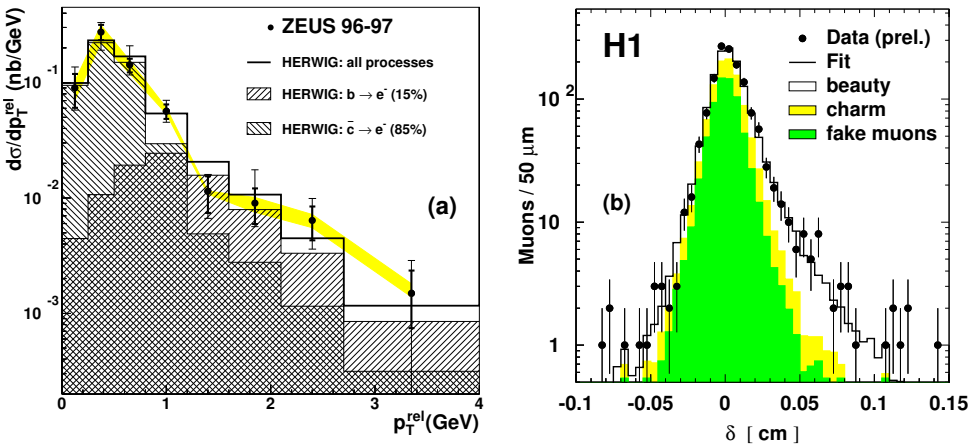

Fig. 15. (a) ZEUS differential cross section for production of an electron with transverse momentum p_T^{rel} relative to the axis of a jet ($E_T > 6$ GeV) in photoproduction. The calorimeter energy uncertainty is shown as a shaded band. The total HERWIG prediction for electron production, and for electron production through $\bar{c}$ and b decays, are indicated. Possible backgrounds from DIS positrons confined the analysis to electrons. (b) H1 measurement of the impact parameter δ of muons relative to the primary event vertex. Two jets of $E_T > 5$ GeV are required.

4. Open Beauty

Both HERA collider experiments have reported measurements of open beauty, i.e. the B family of mesons. The latest H1 results have benefited from the use of a silicon tracking system, and ZEUS will use such a system in future running. In the absence of a precise vertex measurement to help identify the B mesons, with their relatively long lifetime, the most common identification procedure is by means of their leptonic decays. The high mass of the b quark compared with the c means that the B meson decay products emerge at higher angles relative to the direction of outgoing heavy-flavour meson or its jet (fig. 15a).[63] Important backgrounds come from the leptonic decays of D mesons.

ZEUS have used this method to obtain an inclusive B photoproduction cross section, where B denotes all b-quark mesons, taking an inclusive branching ratio to electrons. H1 have useed muons,[64] and have more recently demonstrated the effectiveness of a selection on impact parameter (fig. 15b), presenting preliminary measurements in both photoproduction[65] and DIS.[66]

The results are summarised in fig. 16a. Since the measurements are defined using different experimental acceptances, they are plotted as a ratio of the measured cross sections to the predictions at NLO from the HVQDIS program. A Peterson fragmentation function was used to calculate B production rates, from which lepton cross sections were extracted using the AROMA generator — in other words, a similar method to that used by H1 for their D measurements. The HVQDIS program yielded a predicted cross section of 11 ± 2 pb for the production of B hadrons at HERA, compared with the H1 DIS measurement of $39 \pm 8 \pm 10$ pb. AROMA itself

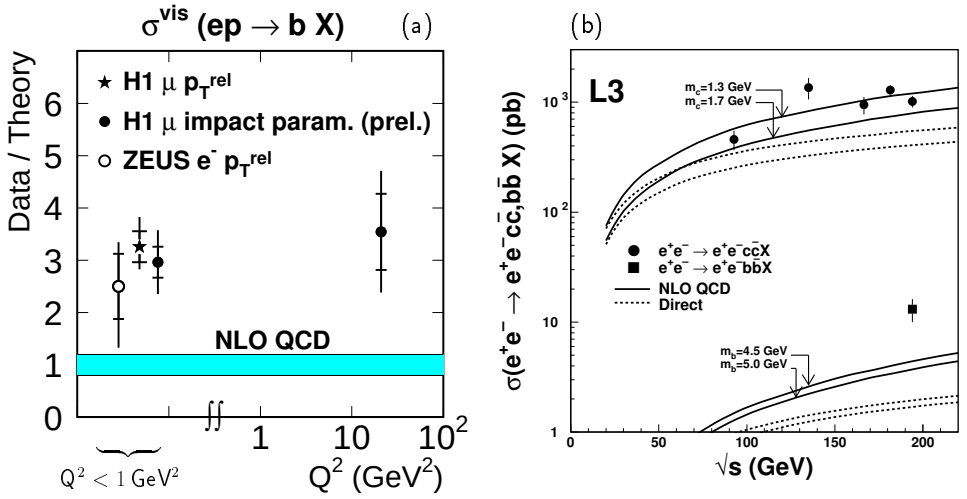

Fig. 16. Open beauty production in various hadronic processes. (a) At HERA using H1 and ZEUS, as a function of Q^2. (b) At LEP using $\gamma\gamma$ collisions with the L3 detector, together with open charm results (upper points and curves). Statistical and systematic uncertainties are added in quadrature.

gives a prediction of 9 pb and CASCADE, at LO, gave 15pb. The photoproduction theoretical result was calculated using the FMNR program.

In short, the integrated B cross sections at HERA lie consistently above the NLO theory whenever the experimental errors permit a statement. It is therefore worth making comparison with results from other types of experiment. At LEP, measurements of charm and beauty production have been made in photon-photon collisions by L3[67] and OPAL.[68] The acceptance is evaluated using PYTHIA and the results compared to NLO predictions from Drees et al.[69] The charm situation is found to be not dissimilar to that at HERA. L3 (16b, top) present charm cross sections in overall accord with calculations, bearing in mind the c mass uncertainty. OPAL, measuring D^* production with p_T between 2 and 12 GeV,[70] find that the massless calculation by Binnewies, Kniehl and Kramer[42,71] fits the data well, while a massive calculation by Frixione, Krämer and Laenen[72] underestimates the data even with $m_c = 1.2$ GeV. The direct process, here referring to $\gamma\gamma \to q\bar{q}$, is insufficient to account for the observed signal, and the authors argue that a resolved photon with significant gluon content is required.

However the beauty rate in L3 is much higher than predicted. The OPAL B cross section, selecting on jets with $E_T > 3$ GeV, is in good agreement with L3, whose kinematics are similar. In $p\bar{p}$ collisions at the Tevatron, CDF and D0 have presented extensive data on B production[73,74] and, again, find that the NLO calculation is an underestimate (fig. 17).[75] However it can be seen that at high p_T the disagreement is less serious, the largest discrepancies bein found at $p_T \lesssim 20$ GeV, roughly where the other experiments have obtained their measurements. This region, then, where

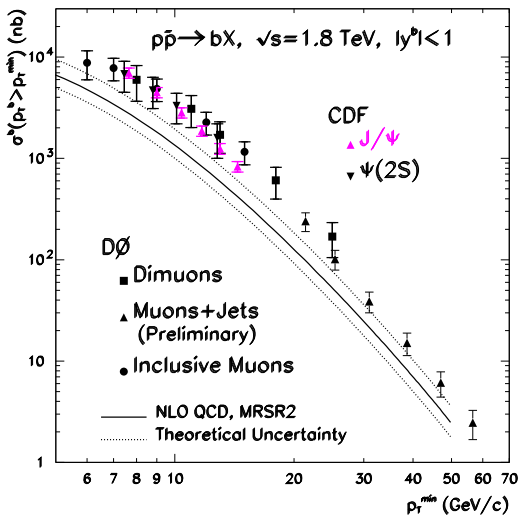

Fig. 17. Beauty production at the Tevatron in CDF and D0, compared with an NLO calculation[75]. The different points denote different ways of identifying b events; the dashed curves indicate the theoretical uncertainty.

the momentum scale of the hard scatter is of the same magnitude as that of the b quark, is where the main trouble seems to lie.

There are suggestions,[76] however, that a full treatment of the excitation and fragmentation contributions within PYTHIA and HERWIG may enable these models to fit the Tevatron b data even at lower transverse momenta. It is important to generate all possible final states where jet fragmentation may produce B mesons. The excitation contributions can be substantial, as indicated in a recent analysis from ZEUS (fig. 18).[77] Although the present experimental errors prevent strong conclusions from being drawn, a large disagreement with theory is not supported by the latter data, although the agreement in the forward direction would be poor without the excitation component.

The value of the b quark mass requires comment. The Particle Data Group[78] quote a value centred on 4.25 GeV at production threshold. In QCD, this mass runs with momentum scale, as confirmed by experiments at LEP.[79] However, programs such as FMNR are based on a different subtraction scheme which requires the "pole" mass, whose value is a little higher, e.g. 4.5 - 5.0 GeV, and is fixed. The Tevatron results are accompanied by an NLO curve calculated with $m_B = 4.75$ GeV^2, and the dashed curves indicate the uncertainties due to the b mass, the renormalisation scale and the Peterson parameter.

Lipatov et al.[80] have discussed BFKL-style models which predict the photoproduction cross section for heavy quark-pair production. The essence of these schemes is to consider alternative types of gluon distribution to those generated by DGLAP evolution. Within the parameter space of this type of approach, these authors are able to account for the H1 beauty cross section as well as for the total charm cross

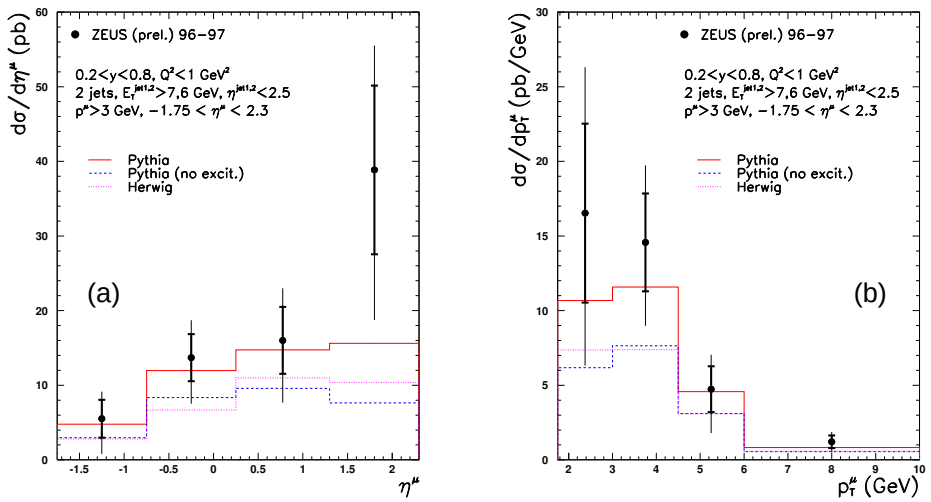

Fig. 18. Results on open photoproduction of beauty (ZEUS, preliminary) compared with predictions of PYTHIA with and without the excitation contribution, and with HERWIG. The B signal is observed in the muonic semi-leptonic decay mode. The experimental cuts are indicated.

sections measured by H1, ZEUS and lower energy experiments. A further account is given by Baranov, Lipatov and Zotov,[81] who demonstrate that such models are able to describe the Tevatron b production cross sections, again provided that suitable variants of the theory are selected.

Although this sounds promising, it is not yet clear that any one implementation of the theory is capable of describing the data from all the experiments. To get the H1 B cross section right, the BFKL model requires a b-quark mass value of 4.25 GeV,[80] which is a little low, while the "semihard" LRSS model[82] is good for both ZEUS and H1, but overshoots the CDF and D0 data if the same parameter set is used. The CASCADE Monte Carlo is able to give a good description of the Tevatron data,[83,23] and, as seen, is fairly satisfactory with ZEUS but not H1. In this model, initial-state gluon radiation gives rise to many low-$x_\gamma^{\rm OBS}$ events. The authors tend to believe that the H1 and ZEUS data are in disagreement.

At present a summary of this fluid situation is difficult: clearly, b-quark production provides an testing-ground for a variety of theoretical ideas. As these develop, and as the experimental errors from H1 and ZEUS decrease, we may expect to achieve serious discrimination between the different approaches.

5. Inclusive Quarkonium Production

The production of $c\bar{c}$ and $b\bar{b}$ mesons has been the subject of extensive study at HERA. Specifically, we are referring to the J/ψ meson (i.e. the $\psi(1S)$ state), the radially excited ψ' (or $\psi(2S)$), and the set of analogous Υ states for the $b\bar{b}$ system. The present section discusses the inclusive production of the J/ψ and $\psi(2S)$ states in photoproduction and DIS. Like the production of open charm and beauty, this

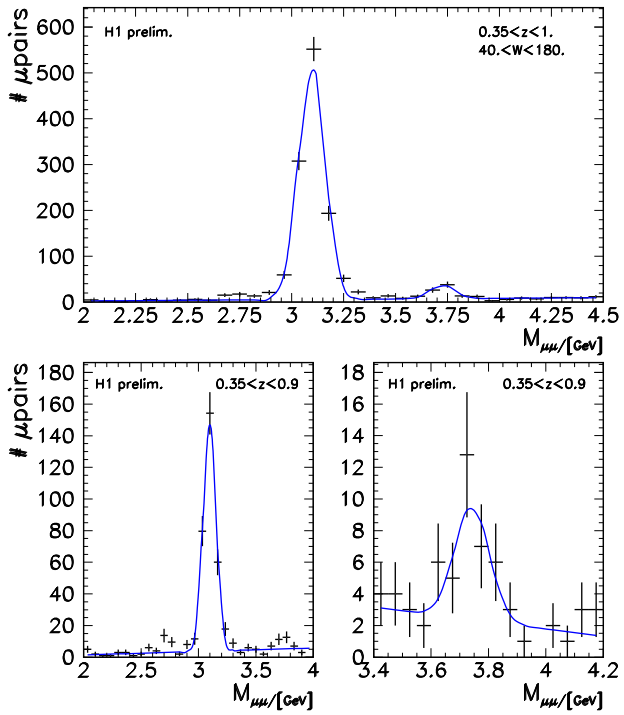

Fig. 19. Dimuon mass spectra in H1 photoproduction.[84] The full 1996-97 data sample is shown (top), followed by the selection used for the inelastic J/ψ measurement and the $\psi'(2S)$ measurement. The γp centre-of-mass energy range is 40 - 180 GeV.

provides an interesting workshop for the study of QCD mechanisms. Experimentally, the J/ψ is conveniently studied at HERA only in its $\mu^+\mu^-$ and e^+e^- decays, but these are fully adequate to identify the particle with reasonable statistics.

The other main area of quarkonium physics at HERA is in the diffractive production of vector states $q\bar{q}$ V through the "elastic" mechanism $\gamma^* p \to Vp$. This will be discussed in Section 6; at HERA, it is only in these processes that the $b\bar{b}$ states have so far been detected.

5.1. *Production of $c\bar{c}$ mesons*

In inclusive $c\bar{c}$ processes at HERA there is no necessity for the bound quark pairs to appear in vector states; however only the vector J/ψ and $\psi(2S)$ states have been actually identified experimentally. Figure 19 illustrates the signals observed in these channels by H1.[84]

As with the production of open heavy quark systems, these processes are modelled theoretically in two stages: (a) a hard QCD subprocess, which is calculable perturbatively and in which the production of the $c\bar{c}$ pair is described, and (b) a soft hadronisation stage where there is a certain probability for a given hadron to

be formed. This may be represented as

$$d\sigma(\gamma^* p \to H\,X) = \sum_n d\sigma(\gamma^* p \to q_h \bar{q}_h(n) + x)\,\mathcal{O}^H(n) \tag{8}$$

in which a series of intermediate $q_h\bar{q}_h$ states, labelled n, are considered, and each has a certain matrix element $\mathcal{O}^H(n)$ for transition into the chosen hadronic state H. The perturbatively calculable subprocess acts at a momentum scale given by the mass of the $q_h\bar{q}_h$ system, or the p_T of the scatter if higher; it is a short-distance, fast process. The intermediate $q_h\bar{q}_h$ system may be in a number of angular momentum states, and is produced in one of two colour states, namely singlet or octet. If necessary, soft gluon radiation ensures the colour-neutrality of the final-state particles.

A specific implementatiion of this scheme uses the so-called non-relativistic QCD or NRQCD approach.[85,86] The initial QCD calculation having first been performed, this effective field theory model allows the $\mathcal{O}^H(n)$ factors to be expressed in terms of known powers of v, the velocity of the heavy quark in the quarkonium system, which should not be too large. The matrix elements are otherwise not calculable from first principles. However, they should be independent of the original QCD process that formed the $q\bar{q}$ state, and the hope is that by measuring experimental cross sections in one context we can obtain information on $\mathcal{O}^H(n)$ terms which can be applied in another.

The chief experimental questions at HERA concern:

- The relative importance of the colour-octet state, or even whether it is important at all;
- The effective value of the mass of the c quark;
- The need for higher-order QCD calculations.

There are expectations that the method will work better for $b\bar{b}$ systems than $c\bar{c}$ systems since the non-relativistic approximations will be more accurate.

Further details have been given by Frixione et al.[18] and in an extensive review by Krämer.[87] This is a situation where several QCD momentum scales apply in the same event, and in particular it is assumed that $m_q v \gg \Lambda_{QCD}$. In general, the power of v which multiplies the matrix elements depends on the relative size of $m_q v$, $m_q v^2$ and Λ_{QCD}.

The simplest version of these ideas is the *colour-singlet* model, in which colour-octet (CO) terms are neglected, since they are suppressed by a power of v^4 compared to the simplest colour-singlet (CS) term. However they are multiplied by a colour factor of 8 and have a different p_T dependence, so that their unimportance cannot be taken for granted. Theoretically, the octet terms are required in order to remove certain infra-red divergences due to soft gluon emission. For best accuracy, one would wish the sum in (8) to include as many terms as possible. In practice, it is not possible to determine more than a small number of the $\mathcal{O}^H(n)$ factors by experiment, and so the hope is that a model with just a few terms included will be able to test the assumption of their universality to sufficient accuracy to

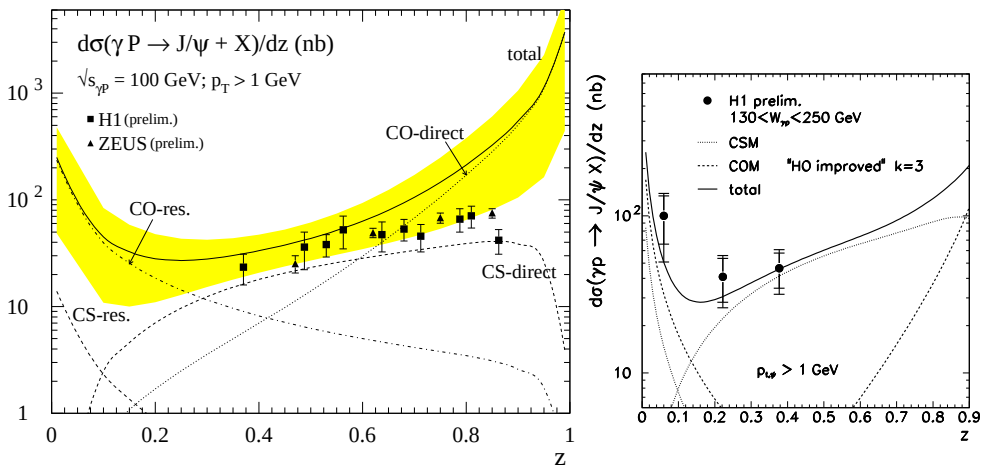

Fig. 20. (left) Experimental data from H1 and ZEUS on inelastic J/ψ photoproduction, compared with theory (Krämer). (right) Data from H1 (preliminary) at low z values.

be useful.[88] The different behaviour of the octet from the singlet terms at large transverse momentum should also provide a useful handle for our understanding of how well these ideas describe the physics.

Both H1[84] and ZEUS[89] have presented measurements of inclusive J/ψ photoproduction. H1 have in addition made the first observations of the ψ' in this channel. Cross sections are given in terms of the p_T of the J/ψ, its centre-of-mass rapidity $y^* = \frac{1}{2}\ln(E+p_z)/(E-p_z)$ and its inelasticity $z = P \cdot P_\psi / P \cdot q$. Here P, P_ψ and q are the four-momenta of the beam proton, the J/ψ and the incident virtual photon. The z parameter is the fraction of the photon energy taken by the J/ψ in the proton rest frame, and is unity for elastic events.

Figure 20(left) shows the cross sections as a function of z, with predictions at LO from the NRQCD model. For $z > 0.3$, the theoretical cross sections are dominated by the direct process, with the CO contribution becoming increasingly dominant as z increases. The CS resolved cross section is small compared to the CO. The shaded band represents the total theoretical uncertainty. The dominant QCD diagram is from photon-gluon fusion, $\gamma g \to c\bar{c}$.

H1 have made a special study[90] of the low-z production of J/ψ's. Figure 20(right) shows results that are in excellent agreement with the LO curves, although the theories quoted here and previously are not identical. The presence of the resolved photon contribution seems clearly required.

It is evident that, while not in disagreement with the LO theory, the data lie at the low edge of the predicted range for CS + CO, and at the high edge (if a similar error band is allowed) for CS alone. The same data are compared to a NLO calculation in fig. 21(a,b), where good agreement is found with a CS prediction alone, although the normalisation uncertainties are again large. The theoretical uncertainties include those on the c quark mass and the QCD coupling constant α_s.

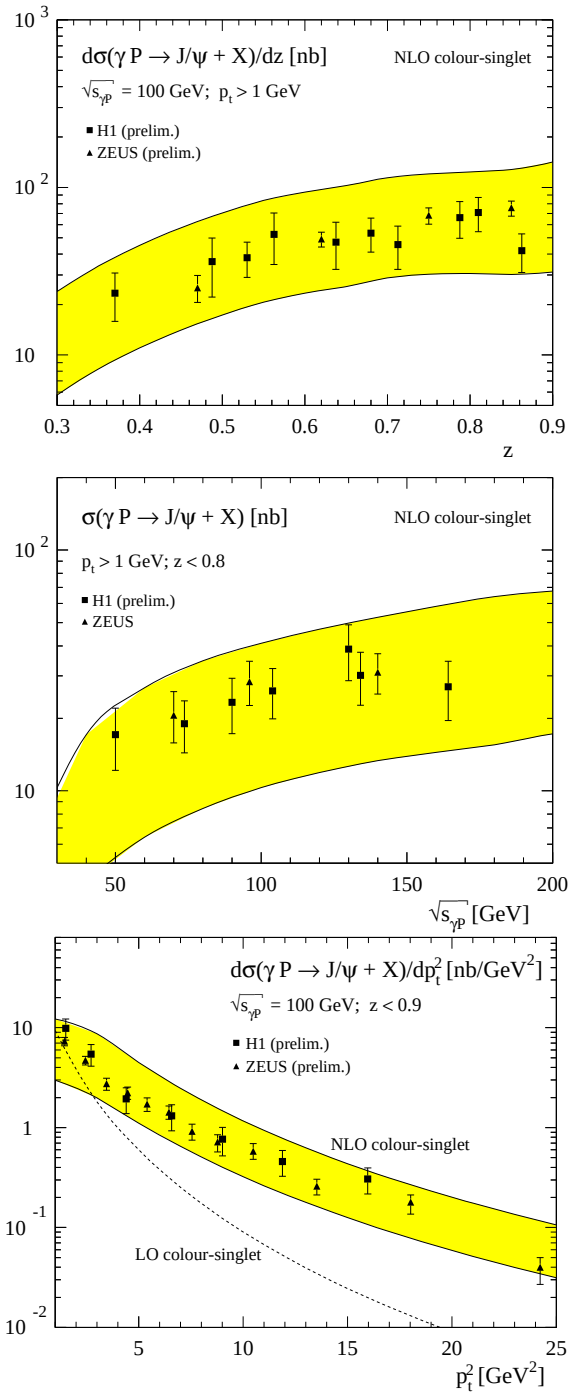

Fig. 21. Experimental data from H1 and ZEUS on inelastic J/ψ photoproduction, compared with NRQCD theory (Krämer)

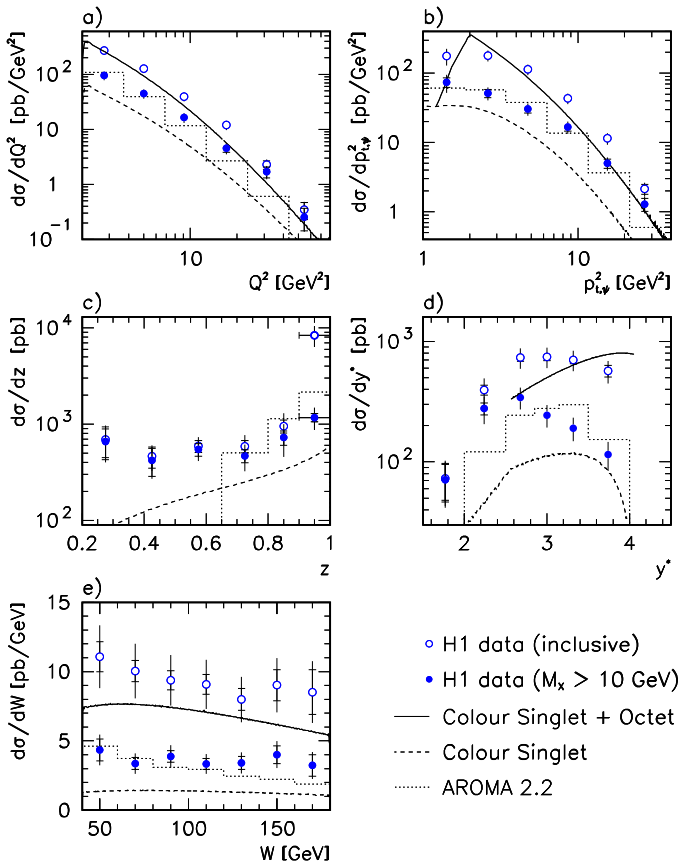

Fig. 22. H1 DIS ep cross sections for various distributions in inclusive J/ψ production (open circles), to be compared with the AROMA histogram, and for inelastic ($M_X > M10\,\mathrm{GeV}$) production (solid circles), to be compared with NRQCD curves from Fleming and Mehen.[93]

ZEUS[89] have also compared their results with a NLO CS calculation[91] and with a LO CS calculation supplemented by a LO CO model using fits from CDF and from CLEO data. The conclusions are similar: NLO CS succeeds, the others sometimes succeed and sometimes fail, but the theoretical uncertainties are large. Clearly, this does not yet amount to a powerful test of these ideas, especially for the presence of the CO term. The p_T distribution (fig. 21c) demonstrates the importance of an NLO calculation. It includes terms which are dominated by t-channel gluon exchange and scale as ${p_T}^6$ instead of ${p_T}^8$, but similar t-channel exchanges occur in the LO CO contribution.

In an analysis of DIS J/ψ production,[92] H1 have presented results with and without a mass cut which effectively removes most events at $z > 0.9$, where the elastic and CO effects are largest (fig. 22). They find that the CO contribution, as calculated by Fleming and Mehen,[93] still dominates the remaining phase space.

Fragmentation is not included in this LO calculation. The CS term is inadequate to describe the data, but including the CO term makes the total too high. H1 attribute these discrepancies to the matrix elements $\mathcal{O}^H$ used in the calculation. Meanwhile the Soft Colour Interaction model,[94] calculated in AROMA, is inadequate at the quantitative level, although the shapes of most of the distributions are described reasonably well.

One path to a better test of these ideas is to measure the polarisation of the J/ψ, where the effects of the CO terms should be more unambiguously visible.[91] It would also be interesting to make an approximate separation between the resolved and direct contributions, by means of x_γ, using the events with a J/ψ jet and a gluon jet.

The production of $\psi'(2S)$ has been measured by H1 relative to that for J/ψ in the same kinematic range of inelastic photoproduction.[84] The cross section ratio was found to be $0.210 \pm 0.048 \pm 0.032$ (preliminary). A substantial fraction of observed J/ψ mesons can be direct or indirect decay products of $\psi'(2S)$ mesons. Allowing for this, H1 calculate the ratio of $\psi'(2S)$ to directly produced J/ψ as 0.24 ± 0.08, in agreement with an expectation of 0.15.[91]

The NRQCD model is itself being developed and studied, with a variety of ideas on the market.[95] These will in due course invite further experimental test.

6. Diffractive Processes

The final topic of this survey concerns the diffractive production of heavy quark systems at HERA. As illustrated in fig. 2d, such processes occur through the photon first fluctuating into a hadronic state V, where V must preserve the quantum numbers of the photon. The assumption of *vector meson dominance* asserts that the relevant hadronic states are the members of the vector meson family, namely the $L = 1$ $q\bar{q}$ mesons ρ, ω, ϕ, J/ψ, Υ etc. The state V may interact inelastically with the proton, but the Optical Theorem requires the existence of an elastic channel, in which the fluctuation $\gamma^* \to V$ is followed by the elastic process $Vp \to Vp$ and the V emerges on mass shell. A full theory must also take into account excitation processes whereby the V or proton may emerge in an excited state.

From a QCD standpoint, the essential feature of diffractive processes is that in the primary scatter, the exchanged object is colour-neutral (colour-singlet). At HERA, this condition permits the proton to remain intact, to end up in an excited nucleon state, or to become dissociated. However there must be no transfer of colour that requires subsequent neutralisation by the generation of a string of hadrons along the rapidity range between the forward nucleon system and the remainder of the event. This rapidity range usually ends up underpopulated or unpopulated, therefore; in fact a so-called "large rapidity gap" is commonly found in the forward region of a diffractive event.

Diffractive processes may be interpreted either in terms of Regge theory, where the exchanged object is a pseudoparticle with the quantum numbers of a vacuum, known as a pomeron, or else in terms of QCD models with the typical exchange of

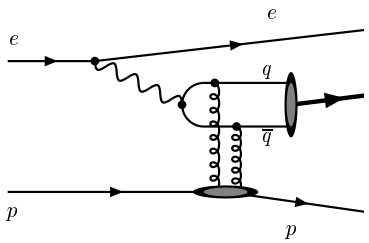

Fig. 23. QCD-modelled production of a vector meson in elastic diffraction (from ZEUS[96]).

two or more gluons (fig. 23). We shall here, for convenience, refer to the exchanged entity generically as a "pomeron".

An account of heavy quark production in diffractive ep scattering must place it against the backdrop of what is now a broad area of "pomeron" physics. Indeed, the manifestations of the pomeron radiated from the proton parallel in many ways the behaviour of the photon radiated from the positron. The pomeron is hadronic, and it may display parton structure and give rise to "resolved" interactions. In the present context, though, we regard it simply as an exchanged object with a possibly complex nature, capable of being modelled in various ways. In the elastic photoproduction of vector mesons the pomeron exchange is a soft process so long as the vector mesons are made of light quarks. However, when $c\bar{c}$ or $b\bar{b}$ mesons are produced, the process cannot be entirely soft from a QCD viewpoint, and so its characteristics change. The situation gives rise to the possibility of perturbative QCD (pQCD) calculations.

In the elastic photoproduction of ρ, ω and ϕ mesons, the fluctuation into a vector meson is taken to occur *before* the scatter off the proton. For the vector meson to remain intact, the scattering process must then be essentially soft. In the QCD-modelled process (fig. 23), the photon couples to a virtual $q\bar{q}$ pair, which exchanges gluons with the proton, and then *finally* the emerging $q\bar{q}$ pair may hadronise into a vector meson. In elastic vector-meson production, the coupling to the proton selects the latter's gluon content at low mean values of Bjorken x. Since $W^2 \propto 1/x$, higher W means lower x, corresponding to a rapidly increasing gluon density in the proton pdf (fig. 13). One expects to observe in general, therefore, that elastic cross sections will increase strongly with W if perturbative QCD is operating. In the Regge approach, a weak rise with W is expected.[97]

Thus the important difference between the elastic photoproduction of light and heavy vector mesons is that the production mechanism of the former is fundamentally "soft" at all stages, whereas the latter require a "hard" phase initially. The situation changes in DIS. The elastic formation of even a light vector meson from an incoming highly virtual photon, with $Q^2 \gg m_V$ requires a hard vertex somewhere, which renders the process in part perturbatively calculable while depressing the cross section.

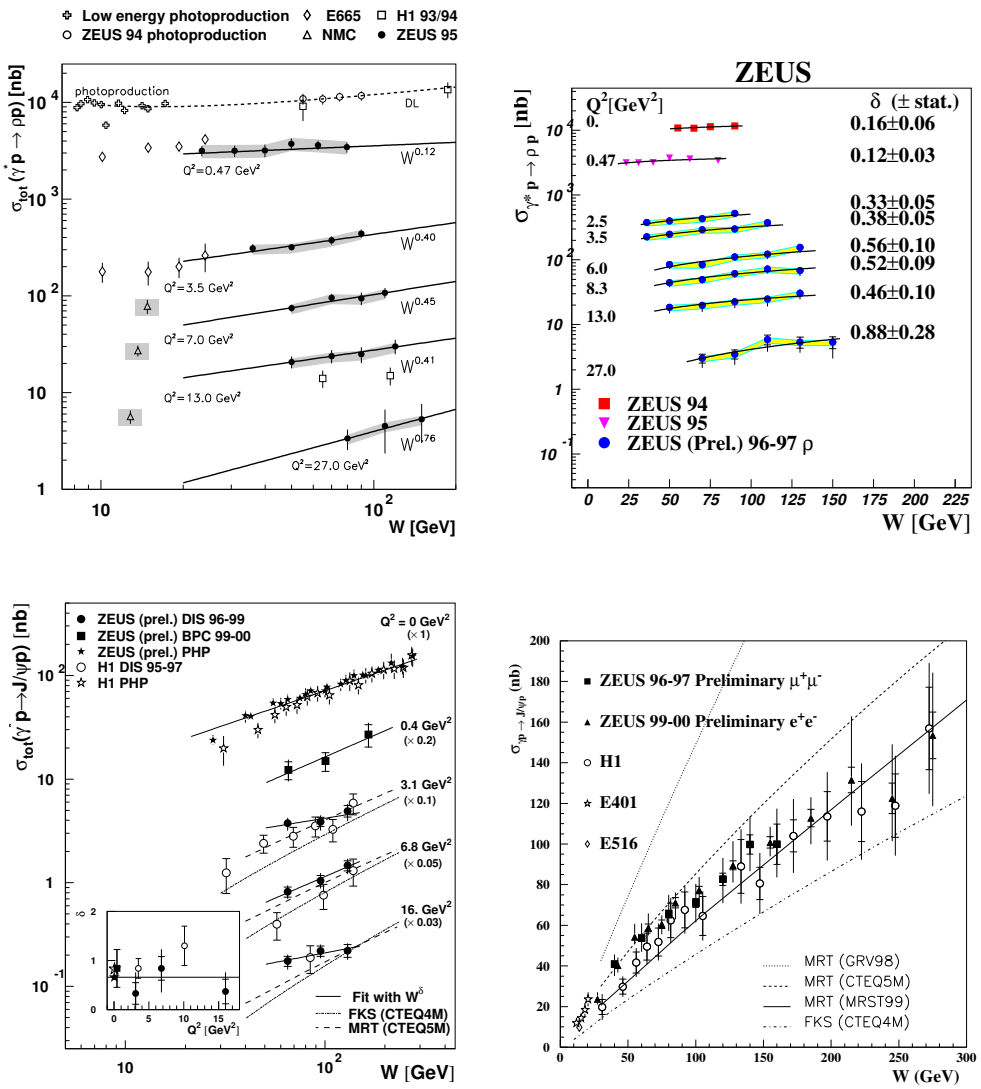

Fig. 24. Total cross sections for $\gamma^* p \to \rho p$ (top)[96,98] and $\gamma^* p \to J/\psi p$ (bottom),[99,101] as measured by ZEUS and H1 as a function of γp centre-of-mass energy and for different values of photon virtuality Q^2. In the first plot, earlier ZEUS data is compared with earlier experiments. The inset in the third plot shows the variation of the parameter δ with Q^2. In the final plot the photoproduction data are compared with pQCD predictions using different proton pdf's in two theoretical models.

6.1. *Measurements of vector charmonium*

The interplay of the different hard scales in diffractive vector meson production is illustrated in the sets of total elastic cross sections shown in fig. 24. In the first two plots, earlier[96] and more recent[98] ZEUS results on ρ production as a function of W are compared with H1. In the third plot, J/ψ data are presented.[99] Recent H1 ρ results[100] are in agreement with ZEUS; the agreement seen in the J/ψ case is likewise reasonable. The cross sections are presented for the cases of photoproduction ($Q^2 = 0$) and for DIS at various Q^2 values. At a given value of Q^2 the W-dependence of the total cross sections can be parameterised as W^δ, where δ is a power to be measured experimentally.

In the case of ρ photoproduction, the data over a wide range of W are well fitted by the Regge-theory formalism of Donnachie and Landshoff,[97] and indicate δ values in the range 0.12 to 0.16 at low Q^2. As Q^2 rises, δ increases to values in the range 0.4 to 0.9, but with a large error for the highest Q^2 data set. The J/ψ data sets, in contrast, show a large value of δ already at $Q^2 = 0$. A value of δ in the range 0.6 - 0.8 is indicated, with no evidence from H1 and ZEUS for variation with Q^2. The suggestion is that by the time Q^2 has reached a suitably high value, a common type of hard behaviour may be found in this W range.

In the fourth plot,[101] J/ψ data at $Q^2 = 0$ are combined and compared with pQCD predictions using different proton pdf sets,[102] all of which give good fits to the proton structure function F_2. The data show a clear sensitivity to the pdf set — that is, to its gluon component — and suggest a preference for one of them. However this should be treated with caution since the two models chosen, FKS and MRT,[103,104] have large uncertainties on their normalisation. They differ in their treatment of the gluon distributions in the photon, and in the description of the charmonium state. Overall, these models may be said to confirm the shape of the variation with W, and the general validity of the pQCD approach to this topic. The FKS model describes the data well when renormalised by a factor of ≈ 1.6.

The coupling of the photon to the vector mesons V is through their quarks; the quark content of the ρ, ω, ϕ, J/ψ and Υ mesons predicts total elastic cross sections for $\gamma p \to Vp$ in the respective ratios $1 : \frac{1}{9} : \frac{2}{9} : \frac{8}{9} : \frac{2}{9}$, respectively, if flavour independence otherwise applies. For five quark types, this is referred to as SU(5) symmetry. The $\omega : \rho$ cross section ratio is found to be in good agreement with this prediction, both in photoproduction and DIS.[105]

However at $Q^2 = 0$ both the ϕ and J/ψ cross sections are lower than predicted. This must be attributed to different production mechanisms, even the ϕ being sufficiently heavier than the ρ and ω to follow significantly different dynamics. To expect SU(5) symmetry to hold, we must operate in a kinematic regime where uniform production mechanisms operate, and it would appear necessary that this be either one where all the mechanisms are soft, or one where pQCD applies but quark mass effects are unimportant. In the latter case this means there must be a hard momentum scale considerably greater than Λ_{QCD} and the vector meson masses.

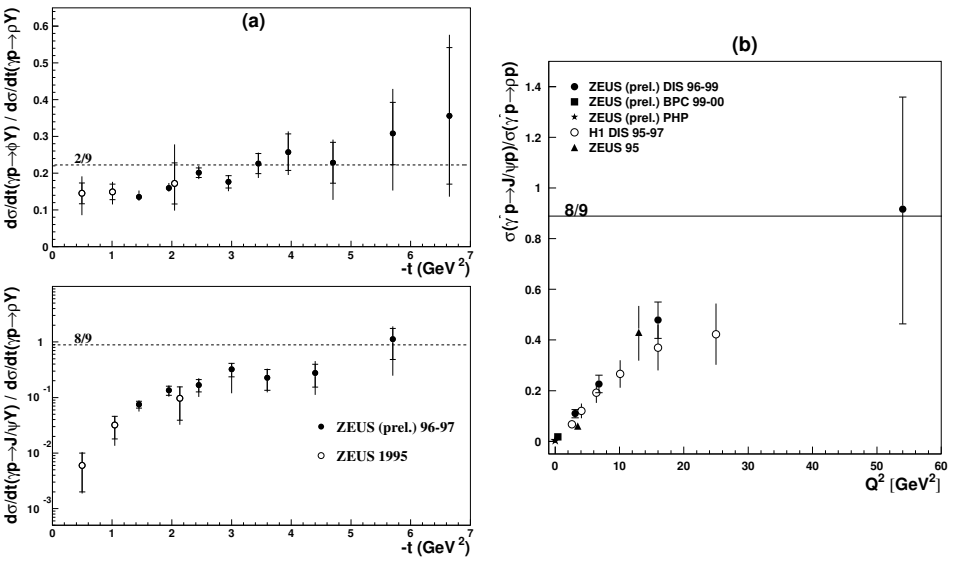

Fig. 25. (a) Ratio of cross sections $d\sigma/dt$ for ϕ and ρ (upper) and for J/ψ and ρ (lower) measured by ZEUS in proton-dissociative elastic scattering $\gamma p \to VY$. (b) Ratio of elastic cross sections for J/ψ and ρ, as a function of photon virtuality Q^2 as measured by ZEUS and H1.

A first area to check is scattering at high momentum transfer t, where ZEUS have measured proton-dissociative diffractive production of vector mesons.[106] The predictions appear to work (fig. 25a): for $|t|$ above approximately 3 GeV or 6 GeV, respectively, the differential cross section ratios $d\sigma/dt(\gamma^* p \to \phi Y) \,/\, d\sigma/dt(\gamma^* p \to \rho Y)$ and $d\sigma/dt(\gamma^* p \to J/\psi\, Y) \,/\, d\sigma/dt(\gamma^* p \to \rho Y)$ become consistent with asymptotic values of 2/9 and 8/9. More high-$|t|$ data are desirable to confirm this to greater precision. The corresponding ratios for the purely elastic ϕ and J/ψ production have also been measured by ZEUS:[107] they are consistent with expectations but the experimental errors are substantial.

Likewise, the total cross section ratio for ϕ relative to ρ plateaus to a ratio of 2/9 when Q^2 exceeds about 6 GeV (which seems to be a higher value than in the case of t, indicating that $-t$ and Q^2 are not equivalent scales).[108,109] For J/ψ, the data are too sparse at present to make a definite statement; however there is a steady rising trend with Q^2, and an asymptotic value of 8/9 is possible (fig. 25b).

H1 have argued[108] (fig. 26) that a universal curve can be plotted through all the total cross sections for $\gamma^* p \to Vp$. The plotted results were taken at a fixed W value of 75 GeV and the different cross section values were scaled by the reciprocal of their respective SU(5) factors, as listed above. (The Υ cross section needed to be extrapolated in W in a possibly questionable way.) After this, a function given by $\sigma_{fit} = a_1(Q^2 + m_V^2 + a_2)^{a_3}$, with suitable values for the constants a_i, passes impressively though the data points.

No explanation was offered by H1 for this observation. ZEUS have studied the

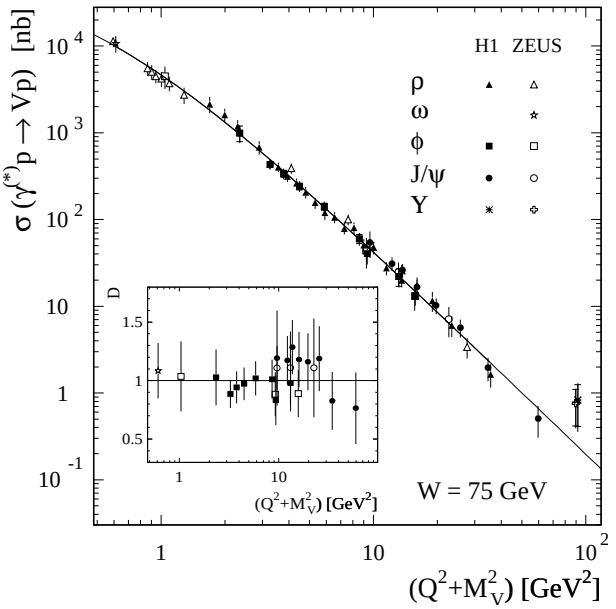

Fig. 26. Total elastic cross sections for vector meson production on a common scale (from H1).

matter further[110] with the conclusion that the postulate of a universal scale variable $(Q^2 + m_V^2)$ is at best an oversimplification. It works for ρ, ω and ϕ production, but fails for J/ψ production when the matter is studied in detail. Taken over a broad W range, and at a series of $(Q^2 + m_V^2)$ values, the scaled J/ψ cross sections are consistently higher by around 50% than the light meson data. At least SU(5) is broken.

As well as scattering elastically in diffractive processes, the virtual photon may dissociate into an unbound $q\bar{q}$ system. ZEUS have presented measurements of D^* production in such processes, both for photoproduction and DIS.[111,112] The kinematical distributions, at present with large errors, are approximately consistent with boson-gluon fusion in resolved-pomeron predictions using RAPGAP.[114] H1 have measured this process in DIS[113] and have obtained satisfactory agreement with QCD model predictions. In both experiments, a suitable parton model of the pomeron is needed, with a dominant gluon component.

6.2. *Regge phenomenology*

The previous sections have treated diffraction principally from a pQCD viewpoint, which has an obvious relevance to heavy quark production. Elastic light vector meson photoproduction is described well within the older Regge framework, however, and this must now be brought into the discussion. A recent account of this area of HERA physics has been given by Abramowicz.[115]

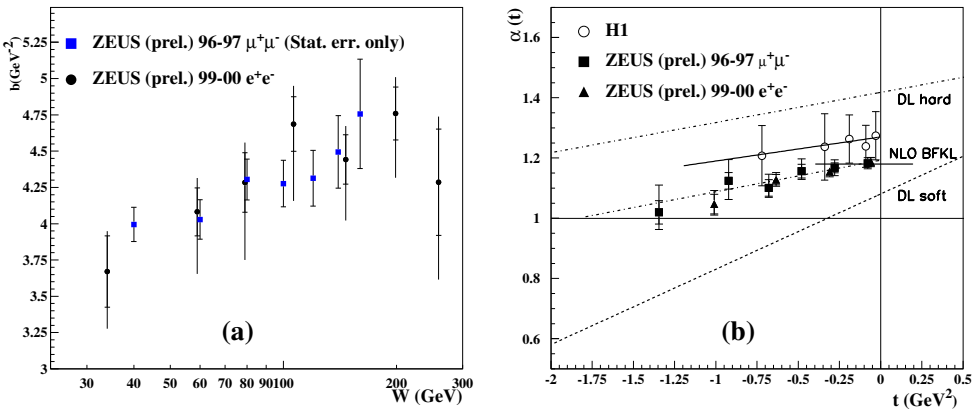

Fig. 27. Elastic scattering parameters b and α in the process $\gamma p \to J/\psi p$ measured by ZEUS (preliminary) and H1.

The differential cross section for Regge pomeron exchange is given by

$$\frac{d\sigma(\gamma p)}{d|t|} \propto \exp^{b_0 t} \left(\frac{W^2}{W_0^2}\right)^{2(\alpha(t)-1)} \tag{9}$$

where $\alpha(t) = \alpha(0) + \alpha' t$. The constants α, α' are believed to be universal, and characteristic of the pomeron, while b_0 and W_0 depend on the particular process. The t distribution depends on

$$b = b_0 + 4\alpha' \ln(W/W_0). \tag{10}$$

A positive value of α' means that the cross section falls more rapidly with $|t|$ as W increases, a characteristic known as "shrinkage". The total elastic cross section, on integrating (9), varies as W^δ where $\delta = 4(\alpha(0) - 1 - \alpha'/b)$. Experimentally one finds $\alpha(0) \approx 1.08$ and $\alpha' \approx 0.25$ GeV^{-2}. Light vector mesons have $b \approx 10$ GeV^{-2}.

There is already a difficulty here in J/ψ photoproduction, because a value $b \approx 4$ GeV^{-2} is measured (fig. 27a), which would give $\delta \approx 0.1$, while the measured value of δ is around 0.8; in other words the actual W dependence is steeper than the Regge formula requires. On the other hand, if pQCD were the whole story, we should not expect to see shrinkage in the J/ψ differential cross section, since in pQCD the W and t dependences are not coupled.[116] From fig. 27b it is evident that shrinkage is indeed observed.[101] This implies non-perturbative physics, which is good news for Regge theory.

Nevertheless, the W dependence represents a problem. In order to rescue Regge theory, Donnachie and Landshoff have proposed a "hard" pomeron[117] as well as the familiar "soft" one which describes light vector meson production well.[118] The hard pomeron has $\alpha(0) \approx 1.4$ while the soft one still has $\alpha(0) \approx 1.08$. However, the experimental t variation gives an intercept of $\alpha(0) = 1.193 \pm 0.011\,^{+0.015}_{-0.010}$. This agrees with a BFKL calculation,[119] but with neither the soft nor the hard pomeron on its own.

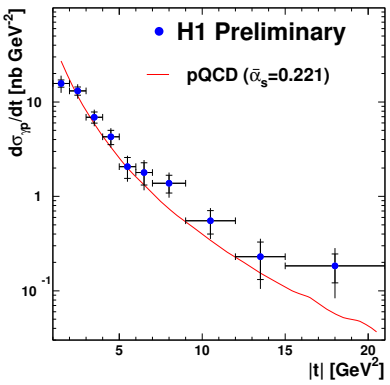

Fig. 28. Differential cross section in $|t|$ for J/ψ production in DIS with proton dissociation (H1). A QCD-based theoretical prediction is shown.

In a more complex approach one may attempt to combine the two types of pomeron. The above authors and H1 have shown that a fit involving both pomerons is able to describe the observed variation of the cross section with W.[118,120] If this is becoming a little complicated, perhaps the pomeron *is* complicated.

One aspect of simple Regge theory which is found to hold in J/ψ production is s-channel helicity conservation (SCHC). This has been reported by ZEUS from an analysis of the relevant spin density-matrix elements using the angular distributions of the J/ψ decay products.[99]

6.3. *Proton dissociation*

In diffractive events at high momentum transfers t, the proton can dissociate while the vector meson still emerges elastically, i.e. with no additional associated final-state products. Recent ZEUS measurements of this process have already been discussed.[106] In J/ψ photoproduction, H1 have made a study[121] selecting events in which the proton dissociates into a final state with a mass in the approximate range 1.6 - 30 GeV, as measured in their forward calorimeter system. The value of t is obtained from the transverse momentum of the measured J/ψ. The pQCD-based event generator HITVM[122] describes the W and the t distributions well (fig. 28). The shape of the variation with t appears to be independent of W; at given t the cross sections rise as W^δ with $\delta \approx 1$.

6.4. $\psi(2S)$ *production*

H1 have measured the elastic production of the $\psi(2S)$ state both in photoproduction and in DIS.[123,92] The decay channel $\psi(2S) \to J/\psi\pi^+\pi^-$ was used, and the results include the contribution from proton dissociation. A colour-dipole based QCD prediction[124] describes the data well (fig. 29). There is also a prediction[116] that for $Q^2 \gg m^2_{J/\psi}$, the ratio of the elastic $\psi(2S)$ and J/ψ cross sections should tend to

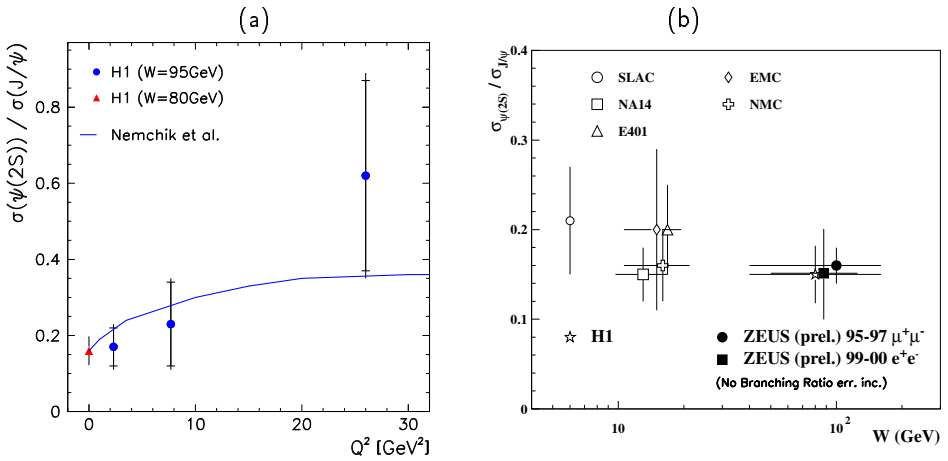

Fig. 29. Differential cross section for $\psi(2S)$ production in DIS with proton dissociation: (a) results from H1 with theoretical comparison, (b) results from ZEUS (preliminary) compared to other experiments.

0.5. ZEUS have measured $\psi(2S)$ production through the e^+e^- decay channel and obtain a result that is consistent with H1 and with lower energy experiments.[125]

6.5. *Measurements of* $b\bar{b}$

The Υ family are the only $b\bar{b}$ states measured at HERA, and have been observed only in the elastic channel in photoproduction and DIS, through their $\mu^+\mu^-$ decays. The dimuon spectrum from H1 is illustrated in fig. 30a.[120] A Υ enhancement is seen with a little difficulty above a background due to the Bethe-Heitler process $\gamma\gamma \to \mu^+\mu^-$, where one of the photons is radiated from the proton. ZEUS have observed a similar signal.[126] The mass resolution is not sufficient to separate the $\Upsilon(1S)$, $(2S)$ and $(3S)$ states, which cover the mass range 9.46 - 10.36 GeV, and so the signal-background subtraction is performed over a range that covers all three resonances together.

The cross section is evaluated assuming that the standard branching rate to muons applies to all three channels and taking 70% of the signal as $\Upsilon(1S)$. The results from the two experiments are shown in fig. 30b, compared with QCD-based calculations by Martin, Ryskin and Teubner (MRT)[104] and by Frankfurt, McDermott and Strikman (FMS).[127] Within present errors, these models all describe the data. A calculation by FKS[103] was found by ZEUS to be too low.

7. Conclusions

The HERA collider offers a rich breadth of perspectives through which many areas of particle physics can be studied, and in so doing stands as an experimental facility unmatched in the world. This is particularly the case in the study of QCD processes, where the production of heavy quark systems provides a laboratory for the probing

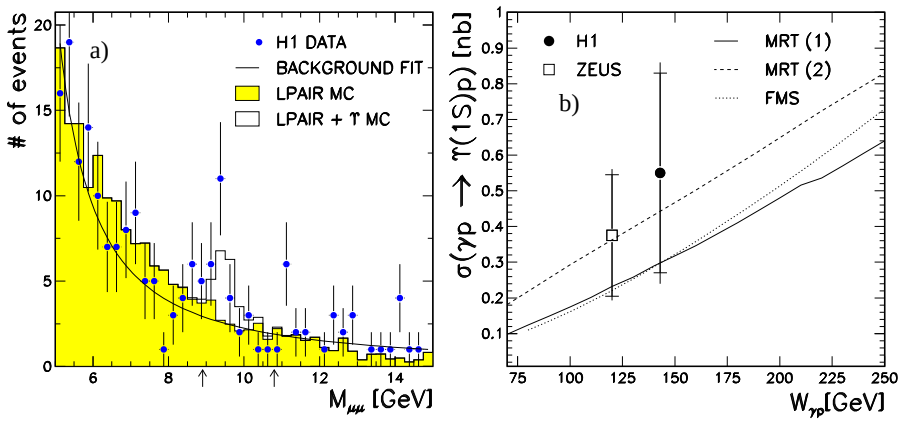

Fig. 30. (a) Dimuon mass distribution in photoproduction from H1. The histogram represents the simulated Bethe-Heitler background. (b) Υ total cross section in photoproduction: HERA results compared to theory.

of many important details of the theory. Mesons containing charm quarks have been extensively measured, and a start has been made on the study of beauty meson production. These measurements have made a useful start in distinguishing between different perturbative and semi-perturbative QCD models. Nevertheless it is clear that better experimental statistics at HERA will be exremely valuable in the study of charm physics, and indispensible for the study of beauty. The ability to study the production of B and Υ mesons at transverse momenta of the same order as the heavy quark mass – yet still "hard" compared with Λ_{QCD} – can give penetrating tests of theoretical ideas.

Although the available energies are not as high as at the Tevatron, and top quark pairs lie outside HERA's reach, the recent improvements to the HERA collider, together with a variety of enhancements in the experiments, make for exciting prospects in this area. Following the machine upgrades, a factor of up to ten in integrated luminosity may be achieved by 2005. No serious evidence against QCD has been found at HERA, but the phenomenological implementations of the theoretical ideas do not yet seem to be perfect. An important onus lies on the theoreticians to provide an understanding of these areas of QCD that will match the quantity and quality of the promised experimental data.

Acknowledgements

I should like to express appreciation of the many fruitful contacts with colleagues in ZEUS and H1 over the years, which have greatly deepened my understanding of QCD physics at HERA, and with particular thanks to D. H. Saxon for a critical reading of the manuscript. I am also grateful to S. Frixione for informative help.

References

1. H1 Collab., *Nucl. Instr. Meth.* **A 386** 310 (1997); *Nucl. Instr. Meth.* **A 386** 348 (1997).
2. ZEUS Collab., M. Derrick et al., *Phys. Lett.* **B293** 465 (1992).
3. G. A. Schuler and T. Sjöstrand, *Nucl. Phys.* **B407** 1993 (539); *Phys. Lett.* B**300** 1993 (169); *Z. Phys.* **C68** 1995 (607).
4. ZEUS Collab., M. Derrick et al., , *Phys. Lett.* **B348** 665 (1995).
5. ZEUS Collab., J. Breitweg et al., *Phys. Lett.* **B413** 201 (1997).
6. J. Huth et al., proc. 1990 DPF Summer Study on High Energy Physics, Snowmass, Colorado, ed. E. L. Berger (World Scientific, Singapore, (1992) 134.
7. H-U. Bengtsson and T. Sjöstrand, *Comp. Phys. Comm.* **46** 43 (1987);
   T. Sjöstrand, *Comp. Phys. Comm.* 82 199474.
8. G. Marchesini et al., *Comp. Phys. Comm.* **67** 465 (1992).
9. C. Peterson et al., *Phys. Rev.* **D27** 105 (1983).
10. P. Nason and C. Oleari, *Phys. Lett.* **B447** 327;
    ARGUS Collab., H. Albrecht et al., *Z. Phys.* **C52** 353 (1991), *Z. Phys.* **C54** 1 (1992) (1999);
    CLEO Collab., D. Bortoletto et al., *Phys. Rev.* **D37** 1719 (1988);
    OPAL Collab., K. Ackerstaff et al., *Eur. Phys. J.* **C1** 439 (1998);
    OPAL Collab., G. Alexander et al., *Z. Phys.* **C72** 1 (1996);
    ALEPH Collab., R. Barate et al., *Eur. Phys. J.* **C16** 597 (2000);
    DELPHI Collab., P. Abreu et al., *Eur. Phys. J.* **C12** 209 (2000).
11. E. Norrbin and T. Sjöstrand, proc. Workshop on Monte Carlo Generators for HERA Physics, 1999, DESY-PROC-1999-02; hep-ph/9905493.
12. H1 Collab., contributed paper 984, XXX Int. Conf. on HEP, Osaka, 2000.
13. ZEUS Collab., J. Breitweg et al., *Eur. Phys. J.* **C12** 35 (2000).
14. G. T. Bodwin and B. T. Harris, *Phys. Rev.* **D63** 077503 (2001).
15. M. G. Bowler, *Z. Phys.* **C11** 169 (1981).
16. V. G. Kartvelishvili et al., *Phys. Lett.* **B78** 615 (1978).
17. P. Collins et al., *J. Phys.* **G11** 1289 (1989).
18. S. Frixione et al., *J. Phys.* **G27** 1111 (2001).
19. V. N. Gribov and L. N. Lipatov, *Sov. J. Nucl. Phys.* **15** 438 (1972);
    L. N. Lipatov, *Sov. J. Nucl. Phys.* **20** 94 (1975);
    Y. L. Dokshitzer, *Sov. Phys. JETP* **46** 641 (1977);
    G. Altarelli and G. Parisi, *Nucl. Phys.* **B126** 298 (1977).
20. M. Ciafaloni, *Nucl. Phys.* **B296** 49 (1988);
    S. Catani, F. Fiorani and G. Marchesini, *Phys. Lett.* **B234** 3 (1990)39 and *Nucl. Phys.* **B336** 1 (1990)8;
    G. Marchesini, *Nucl. Phys.* **B445** 49 (1995).
21. E. Kuraev, L. N. Lipatov and V. S. Fadin, *Sov. Phys. JETP* **45** 199 (1977);
    Y.Y. Balitzki and L.N. Lipatov, *Sov. J. Nucl. Phys.* **28** 822 (1978).
22. H. Jung, proc. Workshop on Monte Carlo Generators for HERA Physics, 1999, DESY-PROC-1999-02, p75 and hep-ph/9908497;
    H. Jung and G. Salam, *Eur. Phys. J.* **C19** 351 (2001).
23. L. Lönnblad, proc. DIS 2001, Bologna (World Scientific, to be published).
24. CTEQ Collab., H. Lai et al., *Eur. Phys. J.* **C12** 375 (2000).
25. A. D. Martin, R. G. Roberts, W. J. Stirling and R. S. Thorne, *Eur. Phys. J.* **C18** 117 (2000);
    R. S. Thorne, proc. DIS 2001, Bologna (World Scientific, to be published); hep-ph/0106075,

A. D. Martin et al., *Eur. Phys. J.* **C14** 113 (2000);
A. D. Martin et al., *Nucl. Phys. (Proc. Suppl.)* **79A** 105 (2001).
26. H1 Collab., C. Adloff et al., *Eur. Phys. J.* **C21** 33 (2001).
27. ZEUS Collab., S. Chekanov et al., , *Eur. Phys. J.* **C21** 443 (2001);
M. Botje, *Phys. Lett.* **B472** 175 (2000).
28. M. Glück, E. Reya and A. Vogt, *Phys. Rev.* **D46** 1973 (1992).
29. L. E. Gordon and J. K. Storrow, *Z. Phys.* **C56** 307 (1992), *Nucl. Phys.* **B489** 405 (1997). *Phys. Rev.* **D45** 3986 (1992).
30. P. Aurenche, J. P. Guillet and M. Fontannaz, *Z. Phys.* **C64** 621 (1994).
31. G. Schuler and T. Sjöstrand, *Phys. Lett.* **B376** 193 (1996).
32. A. Vogt, proc. Workshop on Two-Photon Physics at LEP and HERA, Lund 1994.
33. ZEUS Collab., contributed paper 497, Int. Europhys. Conf. on HEP, Budapest, 2001.
34. ZEUS Collab., contributed paper 501, Int. Europhys. Conf. on HEP, Budapest, 2001.
35. OPAL Collab. K. Ackerstaff et al., *Eur. Phys. J.* **C5** 1 (1998);
ALEPH Collab. R. Barate et al., *Eur. Phys. J.* **C16** 597 (2000).
36. ZEUS Collab., J. Breitweg et al., *Phys. Lett.* **B481** 213 (2000).
37. CLEO Collab., J. P. Alexander et al., *Phys. Lett.* **B303** 377 (1993);
OPAL Collab., K. Ackerstaff et al., *Z. Phys.* **C76** 425 (1997).
38. ZEUS Collab., contributed paper 854, XXX Int. Conf. on HEP, Osaka, 2000.
39. ZEUS Collab., J. Breitweg et al., *Eur. Phys. J.* **C6** 67 (1999).
40. S. Frixione, M. L. Mangano, P. Nason and G. Ridolfi, *Phys. Lett.* **B348** 633 (1995);
S. Frixione, P. Nason and G. Ridolfi, *Nucl. Phys.* **B454** 3 (1995); proc. DIS 2001, Bologna (World Scientific, to be published).
41. B. A. Kniehl, G. Kramer and M. Spira, *Z. Phys.* **C76** 689 (1997);
J. Binnewies, B. A. Kniehl and G. Kramer, *Z. Phys.* **C76** 677 (1997).
42. J. Binnewies, B. A. Kniehl and G. Kramer, *Phys. Rev.* **D58** 014014 (1998).
43. M. Cacciari and M. Greco, *Z. Phys.* **C69** 459 (1996);
M. Cacciari et al., *Phys. Rev.* **D55** 2736 (1997).
44. M. Cacciari and M. Greco, *Phys. Rev.* **D55** 7134 (1997).
45. S. Frixione, M. Cacciari and P. Nason, hep-ph/0107063,
46. H1 Collab., C. Adloff et al., , *Nucl. Phys.* **B545** 21 (1999).
47. A. V. Berezhnoy, V. V. Kiselev and A. K. Likhoded, hep-ph/9901333; *Phys. Atom. Nucl.* **63** 1595 (2000); *Yad. Fiz.* **63** 1682 (2000);
A. V. Berezhnoy and A. K. Likhoded, hep-ph/0005200;
48. ZEUS Collab., contributed paper 499, Int. Europhys. Conf. on HEP, Budapest, 2001.
49. G. Ingelman et al., *Phys. Rev.* **D47** 4872 (1993), *Z. Phys.* **C73** 505 (1997);
U. Karshon, private communication.
50. G. Ingelman, J. Rathsman and G. A. Schuler, *Comp. Phys. Comm.* **82** 74 (1994).
51. B. W. Harris and J. Smith, *Phys. Rev.* **D57** 2806 (1998).
52. H1 Collab., contributed paper 945, XXX Int. Conf. on HEP, Osaka, 2000.
53. S. Riemersma, J. Smith and W.L. Van Neerven, *Phys. Lett.* **B347** 143 (1995).
54. ZEUS Collab., contributed paper 493, Int. Europhys. Conf. on HEP, Budapest, 2001.
55. ZEUS Collab., contributed paper 495, Int. Europhys. Conf. on HEP, Budapest, 2001.
56. M. Aivazis, J. Collins, F. Olness and W-K. Tung, *Phys. Rev.* **D50** 3102 (1994).
57. J. Collins, *Phys. Rev.* **D58** 094002 (1998).
58. J. Amundson, C. Schmidt, W-K. Tung and X. Wang, *J. High En. Phys.* **0010** 031 (2000).
59. A. Chuvakin, J. Smith and B. W. Harris, *Eur. Phys. J.* **C18** 547 (2001).
60. M. Buza, Y. Matiounine, J. Smith and W. L. van Neerven, *Eur. Phys. J.* **C1** 301 (1998).
61. A. Chuvakin, J. Smith and W. L. van Neerven, *Phys. Rev.* **D61** 096004 (2000)

62. B. W. Harris, hep-ph/9909310.
63. ZEUS Collab., J. Breitweg et al., *Eur. Phys. J.* **C18** 625 (2001).
64. H1 Collab., C. Adloff et al., , *Phys. Lett.* **B467** 156 (1999); Erratum (to be published).
65. H1 Collab., contributed paper 979, 982, XXX Int. Conf. on HEP, Osaka, 2000 and Proceedings (F. Sefkow).
66. H1 Collab., contributed paper 807, Int. Europhys. Conf. on HEP, Budapest, 2001.
67. L3 Collab., C. Acciarri et al., *Phys. Lett.* **B503** 10 (2001).
68. OPAL Collab., Á Csilling, proc., Photon 2000, Ambleside; hep-ex/0010060.
69. M. Drees et al., *Phys. Lett.* **B306** 371 (1993).
70. OPAL Collab., G. Abbiendi et al., *Eur. Phys. J.* **C16** 579 (2000).
71. J. Binnewies, B. A. Kniehl and G. Kramer, *Phys. Rev.* **D58** 6110 (1996).
72. S. Frixione, M. Krämer and E. Laenen, *Nucl. Phys.* **B571** 169 (2000).
73. CDF Collab., F. Abe et al., *Phys. Rev. Lett.* **75** 1451 (1995).
74. D0 Collab., A. Abachi et al., *Phys. Rev. Lett.* **74** 3548 (1994).
75. P. Dawson et al., *Nucl. Phys.* **B327** 49 (1988);
    M. Mangano et al., *Nucl. Phys.* **B373** 295 (1992).
76. R. D. Field, private communication.
77. ZEUS Collab., contributed paper 496, Int. Europhys. Conf. on HEP, Budapest, 2001.
78. Particle Data Group, D. E. Groom et al., *Eur. Phys. J.* **C15** 1 (2000).
79. DELPHI Collab., P. Abreu et al., *Phys. Lett.* **B418** 430 (1998);
    ALEPH Collab., R. Barate et al., *Eur. Phys. J.* **C18** 1 (2000);
    A. Brandenburg et al., *Phys. Lett.* **B469** 168 (1999);
    OPAL Collab., G. Abbiendi et al., *Eur. Phys. J.* **C21** 411 (2001).
80. A. V. Lipatov, V. A. Saleev and N. P. Zotov, Mod. Phys. Lett. **A15** 25 (2000).
81. S. P. Baranov, A. V. Lipatov and N. P. Zotov, proc. DIS 2001, Bologna (World Scientific, to be published); hep-ph/01060229.
82. L. V. Gribov, E. M. Levin and M. G. Ryskin, *Phys. Rev.* **100** 1 (1983);
    E. M. Levin et al., *Sov. J. Nucl. Phys.* **53** 657 (1991).
83. H. Jung, hep-ph/0109146.
84. H1 Collab., contributed paper 157aj, Int. Europhys. Conf. on HEP, Tampere, 1999.
85. G. T. Bodwin, E. Braaten and G. P. Lepage, *Phys. Rev.* **D51** 1125 (1995); Erratum, *Phys. Rev.* **D55** 5853 (1997);
    M. E. Luke, A. V. Manohar and I. Z. Rothstein, *Phys. Rev.* **D61** 074025 (2000).
86. W. E. Caswell and G. P. Lepage, *Phys. Lett.* **B167** 437 (1986).
87. M. Krämer, *Prog. Part. and Nucl. Phys.,* (to be published); hep-ph/0106120.
88. G. Schuler, *Eur. Phys. J.* **C8** 273 (1999).
89. ZEUS Collab., contributed paper 851, XXX Int. Conf. on HEP, Osaka, 2000.
90. H1 Collab., contributed paper 988,989, XXX Int. Conf. on HEP, Osaka, 2000.
91. M Krämer, *Nucl. Phys.* **B459** 3 (1996);
    M. Krämer et al. *Phys. Lett.* **B348** 657 (1995).
92. H1 Collab., C. Adloff et al., *Eur. Phys. J.* **C10** 373 (1999).
93. S. Fleming and T. Mehen, *Phys. Rev.* **D57** 1846 (1998).
94. A. Edin, G. Ingelman and J. Rathsman, *Phys. Rev.* **D56** 7317 (1997).
95. G. A. Schuler, *Int. J. Mod. Phys.* A**A12** 3951 (1997);
    S. Fleming, A. K. Leibovich and I. Z. Rothstein, *Phys. Rev.* **D64** 036002 (2001);
    M. A. Sanchis-Logano, hep-ph/0103140.
96. ZEUS Collab., J. Breitweg et al., *Eur. Phys. J.* **C6** 603 (1999).
97. A. Donnachie and P. V. Landshoff, *Phys. Lett.* **B296** 227 (1992).
98. ZEUS Collab., contributed paper 594, Int. Europhys. Conf. on HEP, Budapest, 2001.
99. ZEUS Collab., contributed paper 559, Int. Europhys. Conf. on HEP, Budapest, 2001.
100. H1 Collab., C. Adloff et al., *Eur. Phys. J.* **C13** 371 (2000).

101. ZEUS Collab., contributed paper 878, Int. Europhys. Conf. on HEP, Budapest, 2001.
102. H. L. Lai et al., *Phys. Rev.* **D55** 1280 (1997);
M. Glück, E. Reya and A. Vogt, *Eur. Phys. J.* **C5** 461 (1998);
H. L. Lai et al., MSU-HEO-903100;
A. D. Martin et al.,*Eur. Phys. J.* **C4** 463 (1998).
103. L Frankfurt, W Koepf and M Strikman, *Phys. Rev.* **D57** 512 (1998).
104. A. D. Martin, M. G. Ryskin and T. Teubner, *Phys. Lett.* **B454** 339 (1999).
105. ZEUS Collab., J. Breitweg et al., PL**B487** 273 (2000).
106. ZEUS Collab., contributed paper 556, Int. Europhys. Conf. on HEP, Budapest, 2001.
107. ZEUS Collab., J. Breitweg et al., *Eur. Phys. J.* **C14** 213 (2000).
108. H1 Collab., C. Adloff et al., *Phys. Lett.* **B483** 360 (2000).
109. H1 Collab., C. Adloff et al., *Z. Phys.* **C75** 607 (1997);
ZEUS Collab., M. Derrick et al., *Phys. Lett.* **B377** 220 (1996);
ZEUS Collab., M. Derrick et al., *Phys. Lett.* **B377** 259 (1996).
110. ZEUS Collab., contributed papers 548, 559, 594, Int. Europhys. Conf. on HEP, Budapest, 2001 : Addendum.
111. I. A. Korzhavina, proc. DIS 2001, Bologna (World Scientific, to be published).
112. ZEUS Collab., contributed paper 489, Int. Europhys. Conf. on HEP, Budapest, 2001.
113. H1 Collab., C. Adloff et al., DESY 01-105, submitted to *Phys. Lett. B.*
114. H. Jung, *Comp. Phys. Comm.* **86** 147 (1995).
115. H. Abramowicz, *Nucl. Phys. (Proc. Suppl.)* **99A** 79 (2001).
116. L Frankfurt, W Koepf and M Strikman, *Phys. Rev.* **D54** 3194 (1996).
117. A. Donnachie and P. V. Landshoff, *Phys. Lett.* **B437** 408 (1998); *Phys. Lett.* **B470** 243 (1999); hep-ph/0105088;
P. V. Landshoff, hep-ph/0106120; *Nucl. Phys. (Proc. Suppl.)* **99A** 311 (2001).
118. A. Donnachie and P. V. Landshoff, *Phys. Lett.* **B348** 213 (1995).
119. S. Brodsky et al., *JETP Lett.* **70** 155 (1999).
120. H1 Collab., C. Adloff et al., *Phys. Lett.* **B483** 23 (2000).
121. H1 Collab., contributed paper 806, Int. Europhys. Conf. on HEP, Budapest, 2001.
122. H. Abramowicz et al., proc. Workshop *Future Physics at HERA*, eds. G. Ingelman et al., DESY 1996679.
123. H1 Collab., C. Adloff et al., *Phys. Lett.* **B421** 385 (1998).
124. B. Z. Kopeliovich and B. G Zakharov, *Phys. Rev.* **D44** 3466 (1991);
B. Z. Kopeliovich et al., *Phys. Lett.* **B324** 469 (1994);
J. Nemchik et al., *Phys. Lett.* **B341** 228 (1994);
J. Nemchik et al., *JETP* **86** 1054 (1998).
125. ZEUS Collab., contributed paper 562, Int. Europhys. Conf. on HEP, Budapest, 2001.
126. ZEUS Collab., J. Breitweg et al., *Phys. Lett.* **B437** 432 (1998).
127. L. Frankfurt, M. McDermott and M. Strikman, *J. High En. Phys.* 021999002.